Fast calcite growth driven by galvanic couples

by

Cade Michael Ifland

B.S., Kansas State University, 2022

A THESIS

submitted in partial fulfillment of the requirements for the degree

MASTER OF SCIENCE

Department of Physics
College of Arts and Science

KANSAS STATE UNIVERSITY
Manhattan, Kansas

2024

Approved by:

Major Professor
Bret N. Flanders

Copyright

Abstract

The mineralization of carbon dioxide into calcite, and other carbonates, is a natural mechanism for carbon sequestration that has stimulated vigorous efforts to engineer carbon-capture solutions. It is known that one can deposit calcite by shifting the pH during electroprecipitation, where an overpotential is applied between the substrate and a counter electrode. This process can occur even without the use of electrochemical instrumentation. The presence of dissimilar metals in a mineral-rich soil causes a galvanic couple to become established when the soil gets wet, thus electro-precipitating carbonaceous salts from the soil-based solution. That said, the viability of electro-precipitation (EP) as a soil-based carbon capture strategy is unexplored. The goal of this research is more general; to measure calcite growth rates under a variety of different growth conditions. This growth can be driven by electroprecipitation, or be undriven growth in supersaturated solutions. To this end, we employ a purpose-built quartz crystal microbalance (QCM) coupled to a long working distance optical microscope; this permits the rapid nucleation of a known mass and number of calcite seeds on QCM plates. By transferring these seeded plates to the solutions we want to investigate, we can normalize the resulting growth rate by the active area of the crystal surface. We found that this normalization procedure works well, and that our growth rates in supersaturation are consistent with prior research. In addition, applied voltages can greatly increase growth rates, and are very effectively generated through galvanic coupling. Finally, we have found that a galvanic couple can be used to electroprecipitate carbonate minerals from water-saturated mineral-rich soil samples.

Table of Contents

List of Figures

List of Tables

Chapter 1

Introduction

Calcite and its carbonate relatives play essential roles in our modern world, having a presence in everyday materials such as toothpaste, concrete, plastics, and paper; however, one of calcite's most critical roles is in making our planet livable. Atmospheric CO_2, which regulates planetary temperature through the greenhouse effect, is at equilibrium with dissolved CO_2 in waters and soils; the resulting precipitation of this CO_2 into carbonate minerals, both organically and inorganically, is a crucial part of the carbon cycle [3][4][5][7]. As a result, calcite precipitation has been studied as a potential method for carbon sequestration [6][8][9][10]. Thus, it is desirable to understand the processes by which calcite forms, as well as the ability to control the rate at which it occurs - the *growth rate*; this is the primary focus of this work.

The growth rates of carbonates are very commonly studied, and a plethora of different methods have been used to do it. Macroscopic methods work by measuring changes in solution properties, such as pH or calcium ion concentration, as mineralization and dissolution occur [13][14][15][16]. This mineralization is often induced by the seeding of supersaturated solutions. On the other hand, microscopic methods make a direct measurement of growth; this is commonly done by the repeated scanning the surface of a growing crystal via atomic force microscopy [11][12][17][18][19][20][21]. This method can yield a lot of information about a single crystal as it grows, and accurately measure the velocities of advancing (or receding) atomic steps. However, the singular crystal may not be representative of all of the crystals in the medium, presenting a challenge when relating the step velocity to the macroscopic growth rate.

Furthermore, due to scan rate limitations, AFM is unsuited to measuring fast growth rates. In recent years, macroscopic growth rates have been quantified by a different method. In 2017, Lammers and co-workers used a quartz crystal microbalance (QCM) to measure the attached crystal mass as a function of time [1]. Since there are multiple separate crystals attached to the sensor, the measured growth rate has a larger sample size and is more representative of all the crystals in the medium. The growth rates they found were consistent with prior work, indicating the viability of measuring calcite growth rates via QCM.

The goal of this work is to measure fast growth rates unsuited to AFM; in particular, fast growth driven by a galvanic couple. To do this, we use a combination of a QCM and a long working distance camera microscope to make simultaneous *in situ* measurements of mass and seed number, which allow us to calculate a growth rate. We then use this procedure to measure growth rates under a variety of influences.

Chapter 2

Theory

2.1 The microscopic growth rate

Crystal growth in a homogeneous supersaturated solution that is free of contaminants is expected, on average, to proceed uniformly at each atomic level growth site with a constant growth rate of $k_+c(a)$. We consider a crystal composed of the single component A, so the chemical reaction describing a growth unit of A joining the crystal is $A_{sol} \leftrightarrow A_{cry}$. k_+ is the forward rate constant for this reaction, and $c(a)$ is the concentration of A at the crystal-solution interface located at position a. The growth rate $k_+c(a)$ has units of $\frac{growth\ units}{unit\ time \cdot growth\ site}$.

2.2 The intensive growth rate

The macroscopic growth rate $\dot{M}$ of the whole crystal, or of a population of many individual crystals, each with numerous growth sites (as typically characterized by a quartz crystal microbalance), is the microscopic growth rate multiplied by the number of growth sites n_{sites} on the active surface area A_{act} of the crystal or crystal population: $\dot{M} = n_{sites} \cdot k_+ \cdot c(a)$. Expressing n_{sites} in terms of the growth site density σ and the active area A_{act}, $n_{sites} = \sigma \cdot A_{act}$ gives an absolute growth rate of:

$$\dot{M} = \sigma \cdot A_{act} \cdot k_+ \cdot c(a) \ , \tag{2.1}$$

where $\dot{M}$ has units of $\frac{growth\ units}{unit\ time}$. As this quantity depends on the size of the system (through A_{act}), it will increase in time as the system grows. This expectation suggests normalization by the active area A_{act} to obtain an intensive rate $\bar{R} = \frac{\dot{M}}{A_{act}}$ with units of $\frac{growth\ units}{unit\ time \cdot unit\ area}$:

$$\bar{R} = \sigma \cdot k_+ \cdot c(a) \ . \tag{2.2}$$

This normalized growth rate is expected to be a constant function of time as long as the interfacial growth unit concentration $c(a)$ remains essentially constant. Moreover, if $c(a)$ in Eq. 2.2 equals the bulk growth unit concentration, then the reaction barrier (as characterized by k_+) is the only limitation on growth and the growth rate is said to be reaction-limited. We will illustrate that $\bar{R}$ is maximized and constant in time when growth is reaction-limited.

2.3 The diffusion limitation of growth

To provide a simple picture of how diffusion limitations on the growth rate of a crystal arise, we consider the case of a single spherical crystal of radius a. As this seed grows, the interfacial concentration $c(a)$ may decrease with time due to growth-unit consumption by the crystal. Thus, we need to understand how the diffusion of additional growth units from the bulk solution to the interface affects$c(a)$.

Diffusive flux j_D has units of $\frac{growth\ units}{unit\ time \cdot unit\ area}$, and is defined as $j_D(r) = -D\nabla c(r)$ where D is the diffusivity of the growth unit and $c(r)$ is the growth unit concentration at radial position r in the solution with respect to the center of the spherical crystal. When the rate of

barrier crossing at the interface matches the diffusive current through a concentric spherical shell farther out in solution, the interface is in chemical equilibrium with the surrounding solution [23]. Equating these currents, we obtain $A \cdot j_D = \sigma \cdot A_{act} \cdot k_+ \cdot c(a)$, where $A = 4\pi r^2$ is the surface area of the shell. This relationship can be rewritten as the differential equation:

$$\nabla c(r) = -\frac{k_+ \cdot \sigma \cdot A_{act} \cdot c(a)}{4\pi r^2 D} \ , \tag{2.3}$$

which has the solution

$$c(r) = \frac{k_+ \cdot \sigma \cdot A_{act} \cdot c(a)}{4\pi D} \cdot \left(\frac{1}{a} - \frac{1}{r}\right) + c(a) \ . \tag{2.4}$$

Solving Eq. 2.4 for $c(a)$ by invoking the condition that $c(r = \infty) = c_0$, where c_0 is the bulk concentration, and substituting $A_{act} = 4\pi a^2$ yields

$$c(a) = \frac{c_0}{1 + \frac{k_+ \cdot \sigma \cdot a}{D}} \ . \tag{2.5}$$

Thus, $c(a)$ remains essentially constant so long as $k_+ \cdot \sigma \cdot a \ll D$. Substitution of Eq. 2.5 into Eq. 2.1 gives

$$\dot{M} = \frac{k_+ \cdot \sigma \cdot A_{act} \cdot c_0}{1 + \frac{k_+ \cdot \sigma \cdot a}{D}} \ , \tag{2.6}$$

and dividing by A_{act} yields a normalized growth rate of

$$\bar{R} = \frac{k_+ \cdot \sigma \cdot c_0}{1 + \frac{k_+ \cdot \sigma \cdot a}{D}} \ . \tag{2.7}$$

The two limits of this expression are i*) Purely reaction-limited growth* where $\bar{R} \to k_+ \cdot \sigma \cdot c_0$ when $a \ll \frac{D}{k_+ \cdot \sigma}$, and *ii) Purely diffusion-limited growth* where $\bar{R} \to \frac{D c_0}{a}$ when $a \gg \frac{D}{k_+ \cdot \sigma}$. Since the crystal size a generally increases in time, growth must transition from reaction-limited to

diffusion-limited as the seed approaches a critical size of $a^* = \frac{D}{k_+ \cdot \sigma}$, where $\bar{R}$ has decayed to half its initial value. Eq. 2.7 is plotted in Fig. 2.1, with the critical size marked in red. To quantify this plot, we used $c_0 = 80\ mM$ and $D = 8 \cdot 10^{-12}\ \frac{m^2}{s}$. Reasonable estimates of $k_+ = 1.4 \cdot 10^{-19}\ \frac{m^3}{s}$ and $\sigma = 1.0 \cdot 10^{15}\ \frac{sites}{m^2}$ were taken from Qiu and Orme [2]. We see that $\overline{R}$ remains constant and maximal for seed sizes up to $\sim 1\ mm$. Beyond this value, diffusive limitations become increasingly apparent.

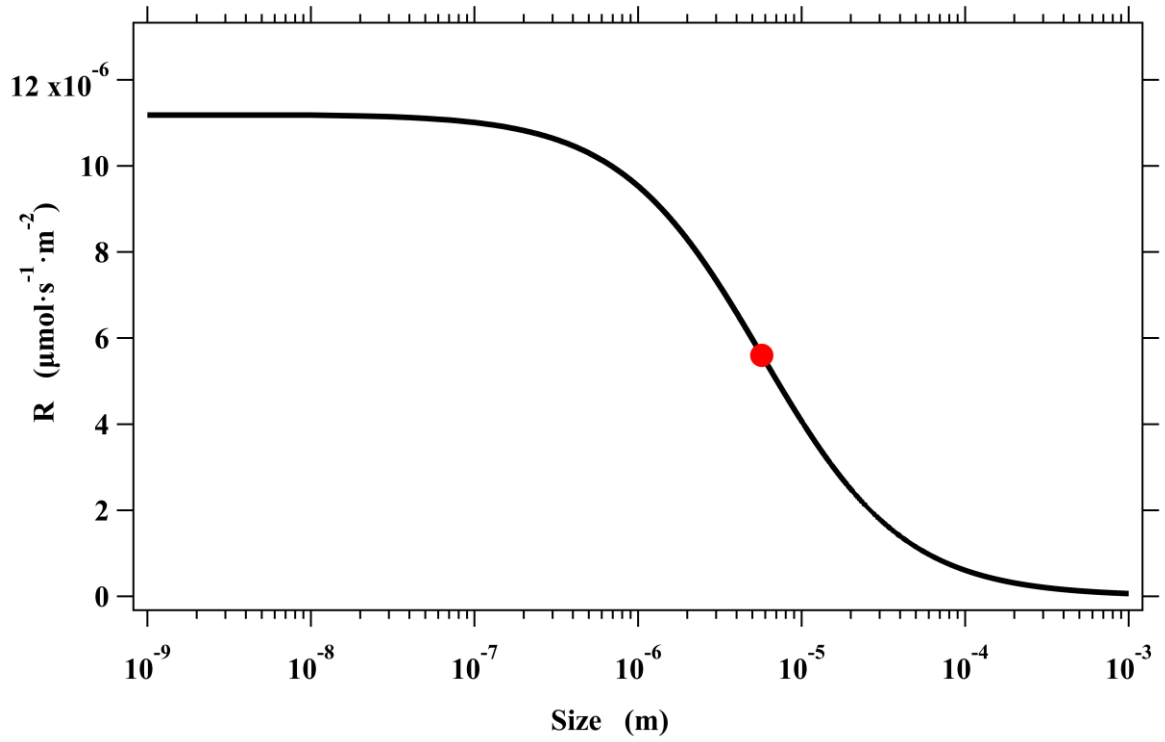

Figure 2.1: $\bar{R}$ versus seed size, as expressed in Eq. 2.7 using the quantities $c_0 = 80mM$, $k = 1.4 \cdot 10^{-19}\ \frac{m^3}{s}$, $\sigma = 1.0 \cdot 10^{15}\ \frac{sites}{m^2}$, and $D = 8 \cdot 10^{-12}\ \frac{m^2}{s}$ [2].

2.4 QCM-derived growth rate

In QCM-based studies of $CaCO_3$ crystallization, the experimental sample typically consists of a large number N of calcite and vaterite crystals on a QCM plate. The QCM measures the total mass of crystal M on the plate as a function of time t, while optical microscopy characterizes the seed-number N. Knowledge of these quantities permits estimation of A_{act} of the N crystals as $A_{act} = c \cdot N^{\frac{1}{3}} \cdot (\frac{M}{\rho})^{\frac{2}{3}}$, where ρ is the mass density of the crystal ($2.71 \cdot 10^6 \ \frac{g}{m^3}$ for calcite) and c is a geometric factor relating surface area to $(\text{volume})^{\frac{2}{3}}$. For a cube, $c = 6$. As differentiation of $M(t)$ gives $\dot{M}(t)$, all parts of $\frac{\dot{M}}{A_{act}}$ can be experimentally determined and the QCM-derived normalized growth rate is

$$\bar{R} = \frac{\dot{M}(t)}{c \cdot N^{\frac{1}{3}}(t) \cdot (\frac{M(t)}{\rho})^{\frac{2}{3}}} \ . \tag{2.8}$$

A challenge with this approach, however, is that numerical differentiation algorithms often introduce uncertainties to data-sets, even after numerical smoothing. Fortunately, there is another way to apply Eq. 2.8 that circumvents numerical differentiation.

For the case of reaction-limited — or even nearly reaction-limited — growth, $\bar{R}$ is essentially constant. Additionally, we have observed that pre-seeding a substrate with N crystals essentially fixes the seed number for the rest of the growth period. So, $N(t)$ is a constant N. When these two conditions are valid, Eq. 2.8 becomes a *homogeneous* differential equation and can be rearranged to $\dot{M}(t) = c \cdot N^{\frac{1}{3}} \cdot \bar{R} \cdot (\frac{M(t)}{\rho})^{\frac{2}{3}}$. Direct integration gives

$$M(t) = \frac{1}{27}(\alpha \cdot t)^3 + \frac{1}{3}m_0^{\frac{1}{3}}(\alpha \cdot t)^2 + m_0^{\frac{2}{3}}(\alpha \cdot t) + m_0 \,, \tag{2.9}$$

where m_0 is the initial mass of the N seeds at time $t = 0\ s$ and $\alpha = c \cdot N^{\frac{1}{3}} \cdot \bar{R} \cdot \rho^{-\frac{2}{3}}$. Thus, Eq. 2.9 permits direct analysis of $M(t)$ data sets without complications from additional numerical errors, provided that growth is reaction-limited and that N remains constant over the growth period. Fig. 2.2 demonstrates the single adjustable parameter ($\bar{R}$) fitting of mass-data (filled red circles) collected by QCM during calcite growth; the solid black line is the fit, and the fitted rate is 6.6 $\frac{\mu mol}{s \cdot m^2}$

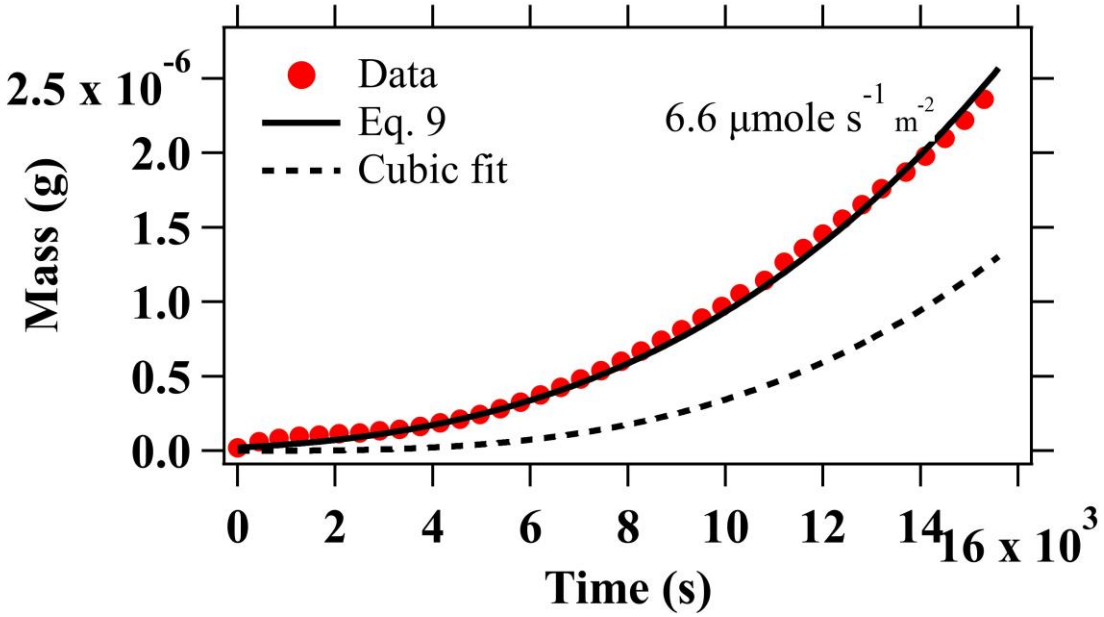

Figure 2.2: Time dependent mass data fitted by Eq. 2.9 using a single adjustable parameter, 6.6 $\frac{\mu mol}{s \cdot m^2}$. The dashed profile is the first (cubic) term of Eq. 2.9, using the same parameters.

When the initial mass m_0 is negligible, Eq. 2.9 shows that the reaction-limited growth of crystals is cubic with time t: $M(t) = (\frac{\alpha \cdot t}{3})^3$. While the cubic growth of calcite is often stated in

the literature, it is a special case. The solid and dashed black profiles in Fig. 2.2 illustrate the difference between the fitted Eq. 2.9 and just its cubic term (when using the same values for N and $\overline{R}$). However, when valid, the cubic growth of the mass implies linear growth of the 1D size. Substituting for k gives $M(t) = N \cdot (\frac{c \cdot \bar{R} \cdot t}{3 \cdot \rho^{\frac{2}{3}}})^3$. Given units of $\frac{mass}{unit\ time}$, dividing by the mass density of the crystal ρ converts mass to volume V; thus, $V(t) = N \cdot (\frac{c \cdot \bar{R} \cdot t}{3 \cdot \rho})^3$. Expressing the total volume of the crystals on the plate by the proportionality $V \propto N \cdot a^3$, where a is the mean size of a single crystal, yields $N \cdot a^3 \propto N \cdot (\frac{\bar{R} \cdot t}{3 \cdot \rho})^3$. Solving for a gives $a(t) \propto \frac{\bar{R}}{3 \cdot \rho} \cdot t$, showing that the reaction-limited cubic growth of mass implies linear growth in the radial dimension.

2.5 Solution design and characterization

Calcite growth in an equilibrated aqueous Ca^{2+}/CO_3^{2-} solution relies on these chemical steps:

$$CO_2(g) \leftrightarrow CO_2(aq) \quad (2.10)$$

$$CO_2(aq) + H_2O \leftrightarrow H_2CO_3 \quad (2.11)$$

$$H_2CO_3 \leftrightarrow H^+ + HCO_3^- \quad (2.12)$$

$$HCO_3^- \leftrightarrow H^+ + CO_3^{2-} \quad (2.13)$$

$$Ca^{2+} + CO_3^{2-} \leftrightarrow CaCO_3 \quad (2.14)$$

$$H_2O \leftrightarrow H^+ + OH^- \quad (2.15)$$

$$K_D = \frac{[CO_2(aq)]}{[CO_2(g)]} \quad (2.16)$$

$$K^{-1} = \frac{[H_2CO_3]}{[CO_2(aq)]} \quad (2.17)$$

$$K_{H_2CO_3} = \frac{[H^+][HCO_3^-]}{[H_2CO_3]} \quad (2.18)$$

$$K_2 = \frac{[H^+][CO_3^{2-}]}{[HCO_3^-]} \quad (2.19)$$

$$Q = \frac{[Ca^{2+}][CO_3^{2-}]}{[CaCO_3]} \quad (2.20)$$

$$K_w = [H^+][OH^-] \quad (2.21)$$

In order to systematically control and quantify the growth rate $k_+c(a)$ of calcite in Ca^{2+}/CO_3^{2-} solutions, we need to prepare solutions of known calcite supersaturation S. S is equivalent to $(\frac{Q}{k_{sp}})$, where Q is defined in Eq. 2.21, and K_{sp} is the equilibrium constant of $CaCO_3$: $K_{sp} = \frac{[Ca^{2+}]_e[CO_3^{2-}]_e}{[CaCO_3]_e}$. Supersaturation is one of many interdependent solution properties, such as pH, temperature, and the solute concentrations, that are related by the chemical equilibrium conditions (Eq. 2.16 – 2.21) and the charge neutrality condition. If enough properties are specified, these equations can be solved to find all solute concentrations and S; we use the software Geochemist's Workbench (GWB) to do this for us. Our Ca^{2+}/CO_3^{2-} solutions are prepared by mixing sodium bicarbonate, calcium chloride, and sodium chloride with deionized water. To design a solution we specify temperature, pH, the initial sodium bicarbonate ($NaHCO_3$), and the ionic strength. We then require that the activities of CO_3^{2-} and Ca^{2+} (both of which comprise a growth unit) be the same at equilibrium. From this, GWB can calculate the concentrations of $CaCl_2$ and $NaCl$ that are necessary to satisfy these requirements, as well as the equilibrium concentrations of the key species, such as $[HCO_3^-]$ and $[CO_3^{2-}]$, and the supersaturation level (S). In Fig. 2.3, S is plotted versus alkalinity; in our system, alkalinity is equal to the original molarity of $NaHCO_3$, and is positively correlated with pH. As you can see, supersaturation varies greatly with the amount of sodium bicarbonate, and as a result pH.

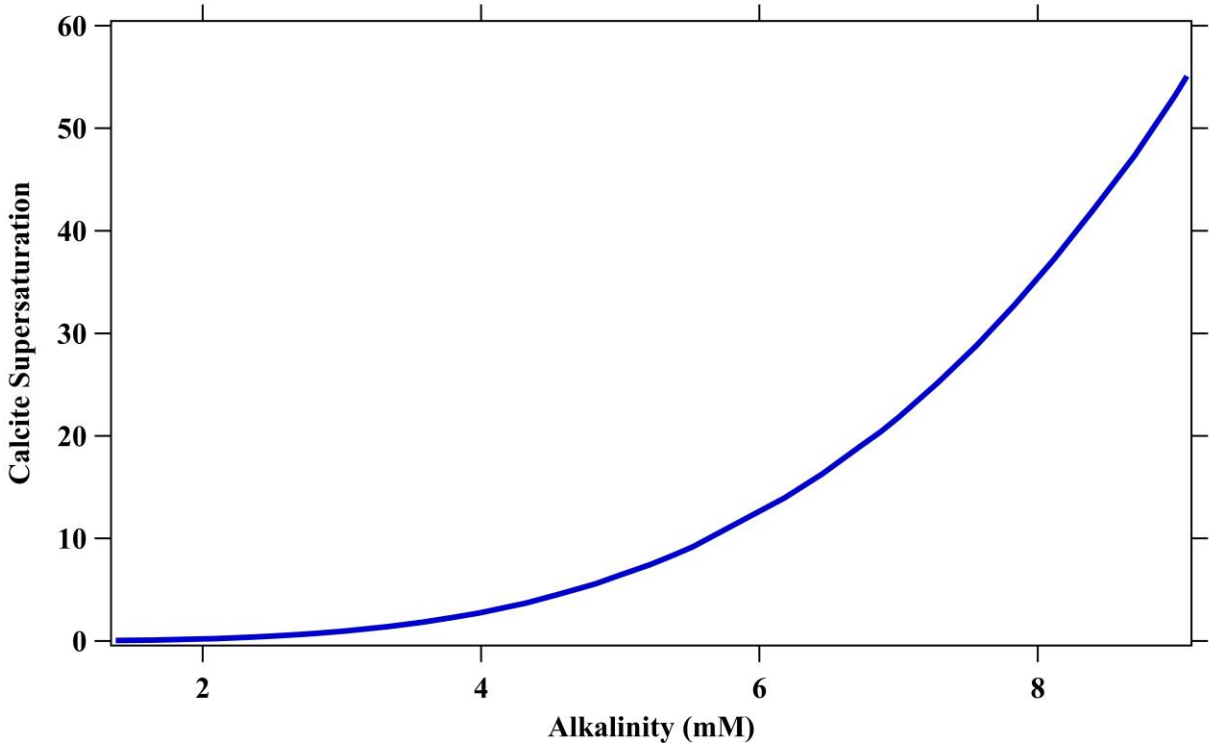

Figure 2.3: *S* versus alkalinity (total sodium bicarbonate content)

Chapter 3

Experimental

Our method for quantifying the growth rates of $CaCO_3$ crystals requires the production of aqueous supersaturated Ca^{2+}/CO_3^{2-} solutions, the use of quartz crystal microbalance (QCM) to measure crystal mass as a function of time, and optical imaging of the QCM plates during and after the nucleation and growth phases of the experiment. A number of properties of the Ca^{2+}/CO_3^{2-} solutions need to be controlled (e.g. supersaturation level), and each growth rate study requires the simultaneous measurement of the crystal mass and the number of crystals on the QCM plate as functions of time. Details on these tasks are provided below.

3.1 Preparation of Ca^{2+}/CO_3^{2-} solutions

To prepare a solution we designed in Geochemist's Workbench, we make two primary solutions (A and B); solution A contains the $CaCl_2$ (CAS 10035-04-8) and $NaCl$ (CAS 7647-14-5), while solution B contains the $NaHCO_3$ (CAS 144-55-8). The molarities of each salt are twice that of the desired solution, such that combining equal quantities of A and B produces the correct molarities. This is done so the primary solutions can be prepared well in advance without risking unwanted crystallization, and then mixed ~15 minutes before use. To make the primary solutions, deionized water (18.2 $M\Omega \cdot cm$) is measured into one-liter glass bottles; salts are measured out (Ohaus Pioneer analytical balance, PA64), and added to the solution. Solutions are

mixed vigorously while open to the atmosphere, so that the dissolved gasses can come into equilibrium with atmospheric levels. This is important as dissolved oxygen is necessary for certain reactions and atmospheric CO_2 is our carbon source (see section 3.4). Finally, before use, the primary solutions are measured out and mixed together gently so as not to induce nucleation. Any adjustments to pH are then made by titration with HCl (CAS 7647-01-0) while the solution is monitored using a benchtop pH meter (Thermo Scientific, Orion Star A211) and pH/ATC probe (Thermo Scientific, 8302BNUMD ROSS). The properties of our solutions are detailed in Table 3.1. The term *balanced solution* refers to solutions that were designed to have equal CO_3^{2-} and Ca^{2+} activities, as described in section 2.5. The term *calcium-rich solution* refers to solutions that contain an excess of Ca^{2+}; these are used in experiments where we increase $[CO_3^{2-}]$ by *electroprecipitation*, described in detail in section 3.4. The term *static solution* refers to a dilute solution, having $S \sim 1$ so that crystals neither grow nor dissolve; it is used for holding crystals in their current state.

	balanced solution	calcium-rich solution	static solution
$CaCl_2\ (mM)$	0.93	4	1
$NaHCO_3\ (mM)$	39.00	4	1
$NaCl\ (mM)$	39.30	0	0
pH	8.25	8.25	8.25
Temperature	22.5° C	22.5° C	22.5° C
Supersaturation	12.5	24.2	2.2

Table 3.1: Properties of our three most commonly used solutions

3.2 Optical characterization of seed beds

To determine crystal growth rates, we need to count the number of calcite crystals, or "seeds" on the QCM plate. This can be done through the direct imaging of the plate's surface, followed by image analysis to yield N.

While many different options for the imaging of a plate surface exist, most are limited in the sense that images of the surface can only be obtained out of solution. As such, we made use of an upright stereo microscope (Leica, S9-D) that has a sufficiently long working distance of $12.2\ cm$ to visualize a mounted QCM plate *in situ*. The optical resolution is $\sim 2.2\ \mu m$ (*i.e.* numerical aperture $= 0.167$). The microscope is equipped with a $12\ MP$ digital camera with $1.5\ \mu m \times 1.5\ \mu m$ pixels (Leica, Flexacam C3). Typical magnifications are in the $30\times - 40\times$ range, so resolution-limited features are comfortably imaged by this camera. Shown in Fig. 3.1 is a seed bed at $55\times$ magnification. As can be seen, these seeds are well defined visually; cubic calcite is present, as well as non-cubic calcite (possibly nailhead).

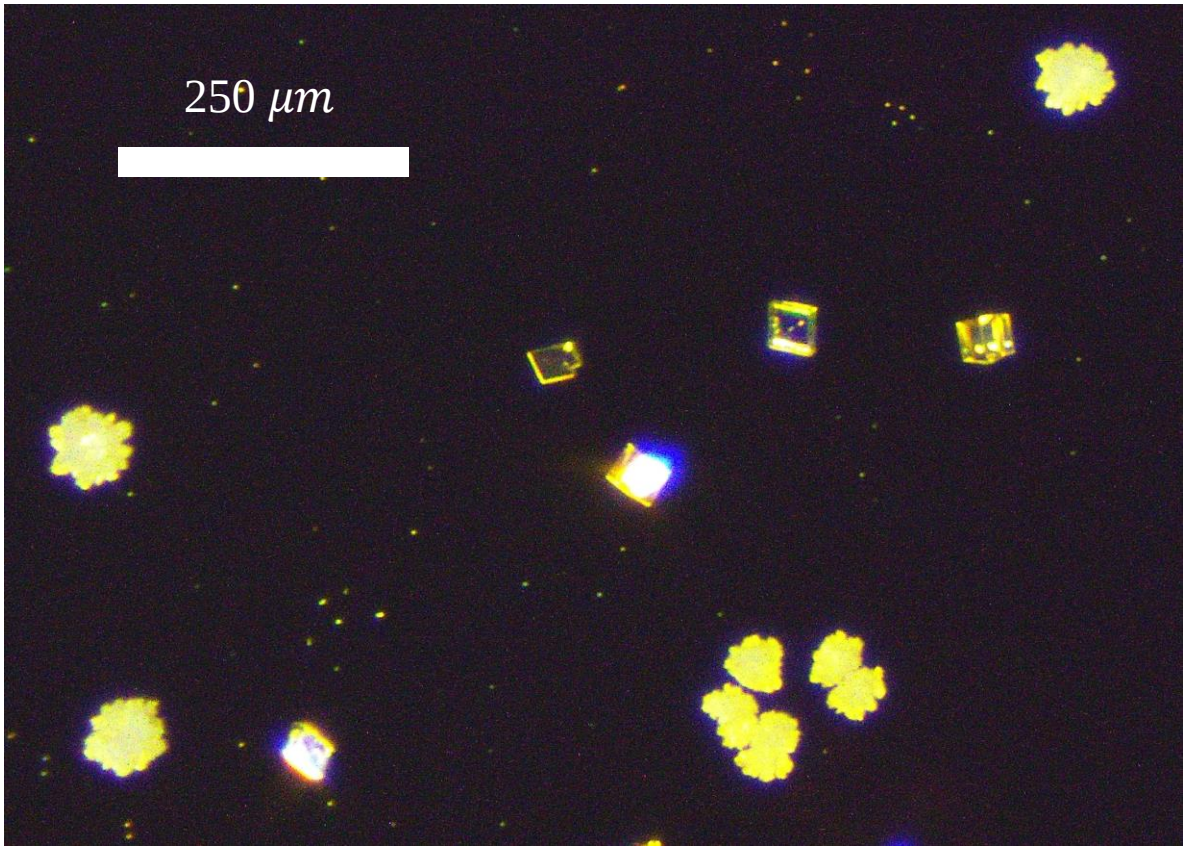

Figure 3.1: Image of calcite crystals taken with S9D at 55 × magnification

As the QCM heads need to be mounted vertically, a 45° mirror and a clear acrylic Roux bottle with an optically flat face facilitate imaging. This setup allows for the real time counting of the seed number N during the seeding process. In conjunction with mass measurements, we can estimate our active area, $A_{act} = c \cdot N^{\frac{1}{3}} \cdot (\frac{M}{\rho})^{\frac{2}{3}}$ in real time. This feedback permits the creation of seed beds having a desired A_{act}, *regardless* of how many nuclei were formed in the nucleation phase. Fig. 3.2 is a diagram showing the key components of our experimental setup for the seeding of QCM plates. The microscope, camera, and mirror work to image the crystal while the QCM measures mass and the potentiostat performs the seeding (details in section 3.4).

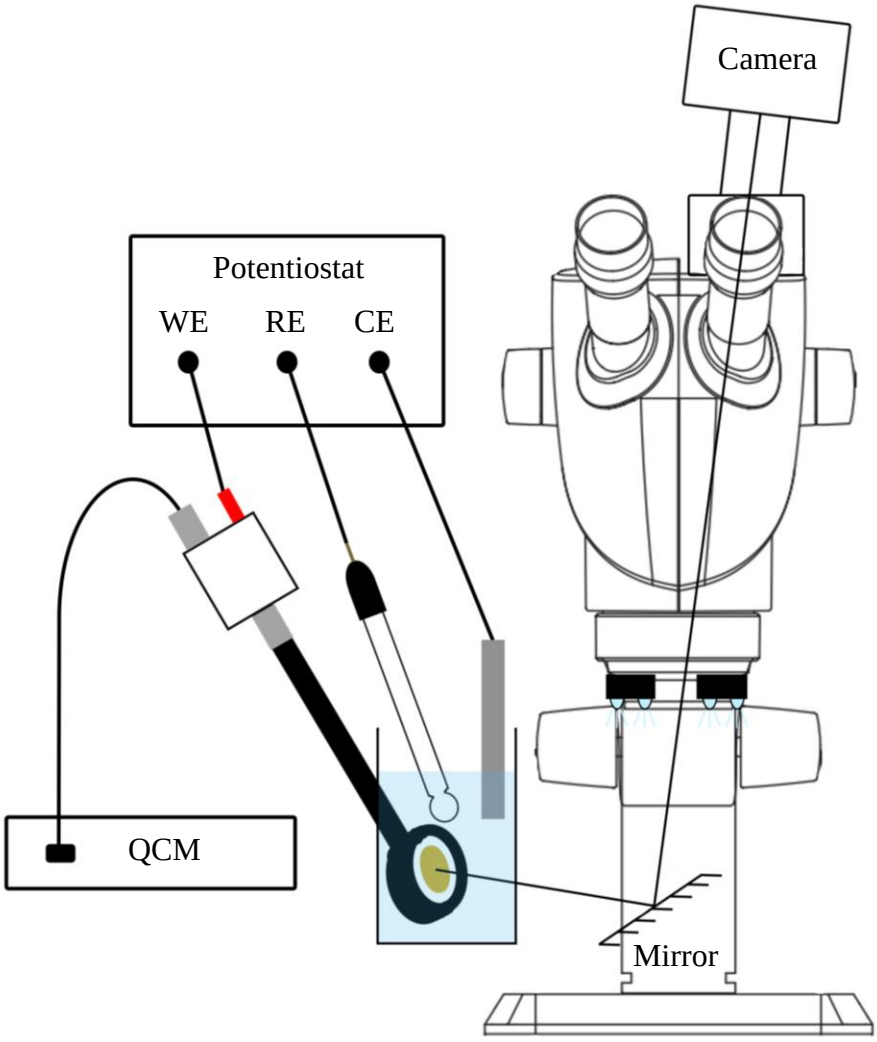

Figure 3.2: Diagram of electroprecipitation setup

The image analysis is a simple yet crucial part of this process. All analysis is done using our own Python code which perform three main operations; *i*) conversion of a color image to greyscale *ii*) binarization of the image based on a brightness threshold value, and *iii*) counting of connected white regions that lie within an acceptable size range. The required brightness, minimum area, and maximum area values to be considered a nuclei are supplied by the user.

Values are chosen such that the relatively bright and homogenous seeds *are* counted, but smaller and dimmer items such as scratches, dust, surface defects, etc. *are not*. A region of a typical analyzed image is shown in Fig. 3.3. The shown area is $\sim .12\ cm^2$, about $1/3$ of the total mass sensitive area of the QCM plate. The 19 seeds that meet the minimum area we specified (55 pixels at a binary threshold of 150) have been highlighted in green.

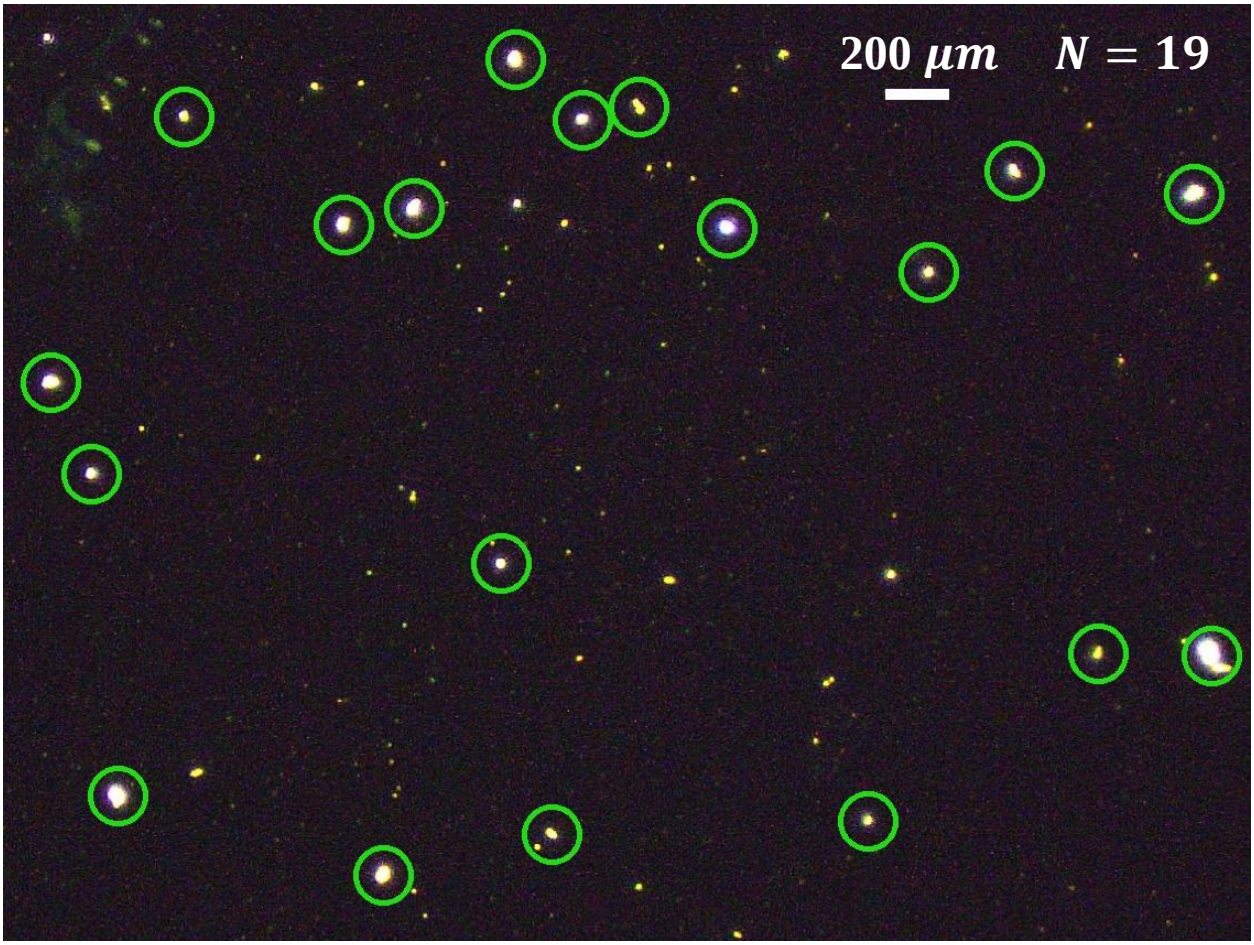

Figure 3.3: Analyzed seed bed, N = 19; nuclei are highlighted in green.

The analysis routine is capable of running while we electroprecipitate seeds onto a plate (detailed in section 3.4). Typically, we observe the optical images of a plate on a large monitor at an imaging rate of ~1 frame per second. The routine reports the seed count of each frame directly

on the displayed image. This feature allows us to monitor the progress of the seeding phase and provides an estimate of the final seed number, which is a useful piece of information in the subsequent growth phase of the experiment. The Python code for this process is provided in Appendix A.

3.3 Mass Measurement

In order to measure $M(t)$ of our seed beds, we utilized a Stanford Research Systems QCM200 quartz crystal microbalance with dispersion. It contains a quartz crystal resonator oscillating at resonant frequency. This frequency, $f(t)$, is highly sensitive to any mass attached to the crystal surface or contact with viscous fluids. Attached mass will shift the resonant frequency according to the Sauerbrey equation: $-C_f \cdot \Delta M = \Delta f$, where C_f is the sensitivity factor of the crystal. The QCM200 has a resolution of 0.1 Hz ($\sim$.7 ng) when a 1 second gate time is used. It should be noted that, due to temperature affecting the solution viscosity, the QCM is sensitive to small temperature changes. Additionally, due to the oscillating nature of the crystal, the QCM circuit is also very sensitive to capacitances. As such, it is critical to balance the QCM via the capacitance compensation knob of the QCM200. In this study, our sensors are 5 MHz AT-cut chromium/gold faced quartz crystals ($C_f = 56.6 \frac{Hz \cdot cm^2}{\mu g}$ at room temp) mounted in a rugged and immersible crystal-holder. The gold working electrode, of which the center .4 cm^2 is sensitive to attached mass, is our interface at which nucleation and then growth occur. Additionally, the QCM200 provides a direct electrical connection to the WE, allowing us to perform the electrochemistry while measuring mass.

To prepare the QCM for use in an experiment, a QCM plate is mounted in the crystal holder, or *head*; This head is placed in a 25% HCl acid solution, rinsed with deionized water, and dried. The head is disassembled, wiped clean with isopropyl alcohol, and left to dry. Meanwhile, a new plate is sonicated for 1 minute in an isopropyl bath, thoroughly rinsed with deionized water, and dried with compressed nitrogen. The plate is plasma cleaned (Harrick Plasma, PDC-32G) on the medium RF level for 3 minutes, and then finally mounted in the QCM head, ready for use.

3.4 Electroprecipitation to create seed beds

The general experimental procedure is to first generate a *seed bed* of calcite crystals with a known N and m_0. The seed beds are then placed in the solution being investigated, and allowed to grow while mass is measured; this $M(t)$ is fit to Eq. 2.9, yielding a growth rate. However, an inherent issue is that nucleation is a random process which happens gradually over time; Eq. 2.9, which requires N seeds to be present at time $t = 0\ s$, is not valid when nucleation occurs gradually. Fortunately, since the propensity for a solution to nucleate is dependent on supersaturation, we can induce nucleation by raising S. S is heavily dependent on pH, as reducing $[H^+]$ increases $[CO_3^{2-}]$. Thus, changes in pH can modulate supersaturation without changing the amount of each salt used to make the solution. A caveat is that an abundance of Ca^{2+} must be present to make use of the increased CO_3^{2-}; to ensure this, our calcium-rich solution contains equal parts $CaCl_2$ and $NaHCO_3$, as mentioned in section 3.1.

The pH can be changed in regions of the solution near an electrode surface via electrochemistry. The application of a potential between two immersed electrodes cause the reduction of oxygen at the cathode;

$$O_2 + 4e^- + 2H_2O \rightarrow 4OH^- \quad 3.1$$

This reduction causes the formation of hydroxide, raising the pH and, as a result, S in the interfacial region of the electrode. This process occurs readily following the application of a negative overpotential, inducing a wave of nucleation over a ~2-minute period. Fig. 3.4 depicts this process. The solid blue line is the frequency shift of the QCM and the solid red line is the number of seeds on the plate. The dashed green, purple, and teal lines mark the times where voltage was applied, nucleation was observed, and mass deposition was observed, respectively. Note that we resolve nuclei optically before we measure any mass; this is due to calcite effectively scattering light.

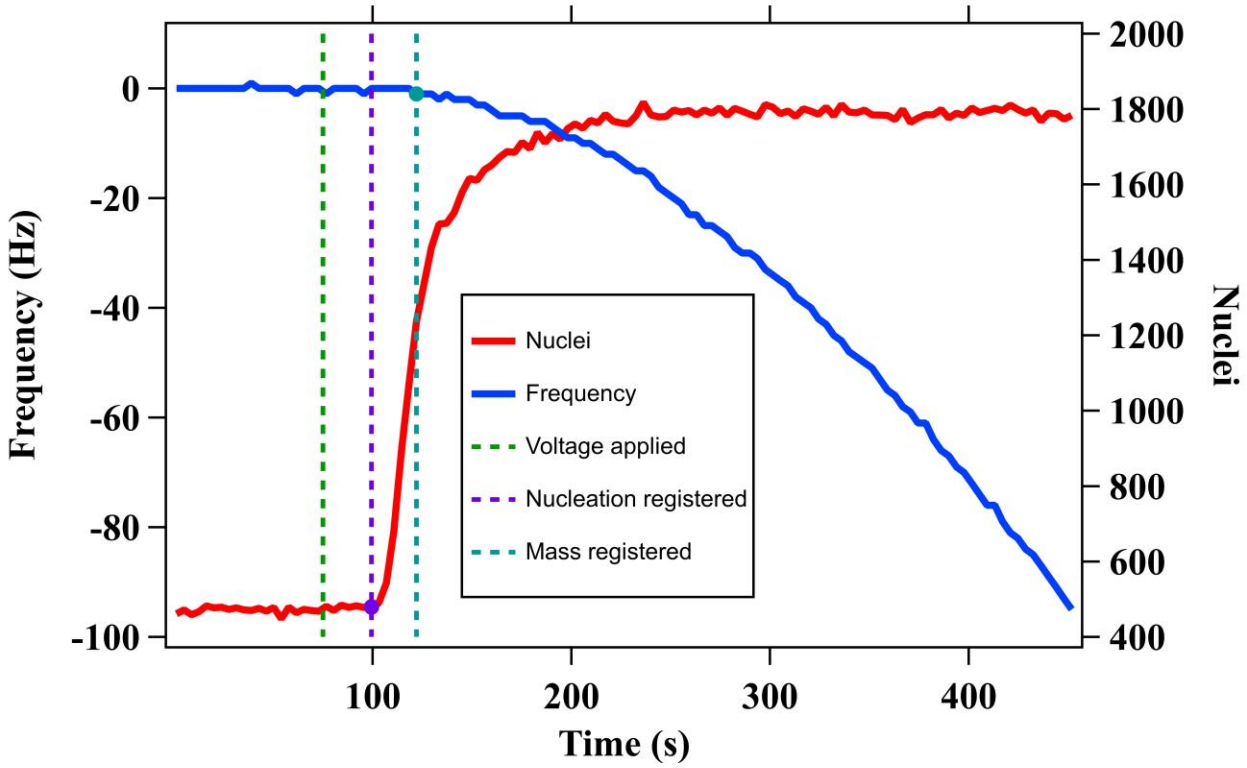

Figure 3.4: Nuclei count and frequency shift (mass) vs time in an EP experiment.

To apply the overpotential, we use a three-electrode system as shown in Fig. 3.2. The working electrode (WE) is the face of our QCM crystal, the reference electrode (RE) is a silver/silver chloride probe, and the counter electrode (CE) is a strip of platinum. The electrodes are connected to a potentiostat, which flows whatever current is required to maintain the RE at a user-supplied command potential relative to the WE. To supply this potential, we use an Agilent 33220A function generator, along with an SRS965 Analog low pass filter to remove all signals except DC.

To prepare a seed bed for a growth study, we place a clean QCM head in the Roux bottle and add 150 ml of calcium-rich solution. Next, we insert the CE and RE and connect the three

electrodes to the potentiostat, which supplies a potential of $0\ V$ to prevent unwanted electroprecipitation. With the microscope focused on the plate surface, we monitor the surface for ~15 minutes while the temperatures of the head and solution equilibrate. Once the temperature, and as a result the QCM, are stable the QCM is balanced and tared. We start the data acquisition program, and allow it to collect data for 75 seconds. Then, we apply a potential of $-450\ mV$ while observing and counting the following nucleation. We allow the seed to grow to a reasonable size (~$5-10\ Hz$ of total mass for a typical experiment), before stopping the program. The head is then rapidly removed from calcium-rich solution, and placed into static solution. This halts the growth and holds the seed bed in an inert state while the growth experiment is prepared.

3.5 Measurement of growth rates

When we measure the growth rate of a solution, we use our seeded plates and QCM200 in conjunction with two water jacketed beakers (Ace Glass, 5340-110). One contains balanced solution for growing the crystal; The other contains static solution for holding the plate (as mentioned in 3.4) and allowing it to reach thermal equilibrium. A water circulator (Fisher Scientific, Isotemp 6200) is used to maintain both solutions at a constant temperature (usually $22.5°C$). For extended experiments, parafilm is used to seal the beaker from the atmosphere and thus prevent pH changes due to gas exchange. The A211 pH meter is used to measure pH before and after the growth period. It can also be used to continuously record $pH(t)$; however, this is not part of our regular procedure due to complications it can introduce, such as poor sealing or difficulty balancing QCM capacitance.

To measure the growth rate, we mix and adjust the solution we are investigating as described in section 3.1, and measure the pH one last time before starting the experiment. We then immerse the recently nucleated and thermally adjusted plate in $200\ ml$ of the solution being investigated. The beaker is sealed, and the QCM is once again balanced and tared. We run our Python code for collecting growth data, as provided in Appendix B. The crystals are allowed to grow for ~2 hours, or until ~500 Hz of mass is deposited. This ensures that the entire reaction-limited regime is recorded, and also makes the seeds prominent and thus easily counted. The plate is removed from solution, rinsed with deionized water, dried with compressed nitrogen, and imaged by the Leica one final time. The pH of the solution is measured again, to verify that it had not significantly changed.

3.6 Driven growth rates

In addition to undriven growth in balanced solution, it is also of interest to measure the driven growth rate. Driven growth is simply growth that is intensified due to electroprecipitation, as described in section 3.4. Depending on what voltage is applied and how that voltage ends up affecting the interfacial pH, a wide range of growth rates can be achieved. Growth can be driven by the same 3 electrode system as in 3.4, at any potential between 0 and $-1.1\ V$; much higher and the water itself is reduced. Growth can also be driven by a galvanic couple; essentially, a metal "driving electrode" which is dissimilar to our gold WE is submerged in solution along with the WE, and the two electrodes are coupled by a wire. The two metals form a galvanic cell, and current flows along the wire; with the right choice of driving electrode, the gold WE will be the

cathode and form OH^-, just like in the three-electrode system. This system is of interest, as galvanic couples in the presence of dissolved carbonates are very common in our soil and water.

Unfortunately, the measurement of driven growth rates is significantly more challenging than that of undriven growth rates. This is primarily because driven growth rates are much faster: $\sim 25 \times$ faster than undriven growth. Revisiting Eq. 2.7, we see that this results in the growth becoming diffusion-limited at a much smaller seed size. This results in a very brief, even nonexistent reaction limited regime. As a result, we often lack enough meaningful data points to fit Eq. 2.9 and thus measure the growth rate. The measurement of the driven growth rate becomes more feasible if a driving electrode made of less reactive metal is used in conjunction with a seed bed composed of small seeds.

To measure a driven growth rate, we mix our solution, adjust the pH of our solution, and immerse the seeded plate in our jacketed beaker, as in section 3.5. Since we are performing electroprecipitation, we use our calcium-rich solution. If being driven by a three-electrode system, the CE and RE are immersed alongside the QCM, and connected to the potentiostat. If being driven galvanically, just the sanded and plasma-cleaned driving electrode is immersed in solution. Care is taken to leave several centimeters of space between the CE or driving electrode and the QCM plate as they can affect the QCM capacitance, making it difficult to balance. These experiments take much less time to grow, so sealing the beaker is not necessary. The QCM is balanced and tared, and the same Python code is executed. After 25 seconds, voltage is applied via either a command potential to the potentiostat, or by bridging the WE to the driving electrode. Growth occurs rapidly, and the seeds are grown to at least $\sim 500\ Hz$. The plate is rinsed, dried, and imaged, and pH is recorded.

Chapter 4

Results and discussion

4.1 Growth rates fit theory well

A key result of our experiments dealing with the undriven growth of seed beds is that the collected $M(t)$ data fits well to Eq. 2.9. Shown in Fig. 4.1 (a) is a typical data set for undriven growth, which was fitted to Eq. 2.9 with $\bar{R} = 7.1\ \frac{\mu mol}{s \cdot m^2}$. This plate was seeded with $N = 1550$ seeds, with an initial total mass of $m_0 = 41\ ng$, and then grown in solution of $S = 12.5$ (details in Table 3.1). The mass data are the blue circles; the fit of Eq. 2.9 to the data is the solid red line. The black circles mark the beginning and end of the region that we fit. As can be seen, the growth agrees with Eq. 2.9 for ~6000 seconds, after which the growth slows; this is what we expect due to the growth becoming diffusion limited. The success of the fitting at early times implies that knowing m_0 and N of a seed bed is sufficient to characterize its growth kinetics by Eq. 2.9, and that growth is indeed reaction-limited at small seed size. These conclusions are important, as they validate the use of Eq. 2.9 to describe the growth of seeded plates.

Fig. 4.1 (b) shows five additional data sets obtained for these same conditions, illustrating typical sample to sample reproducibility of our growth rate measurements.

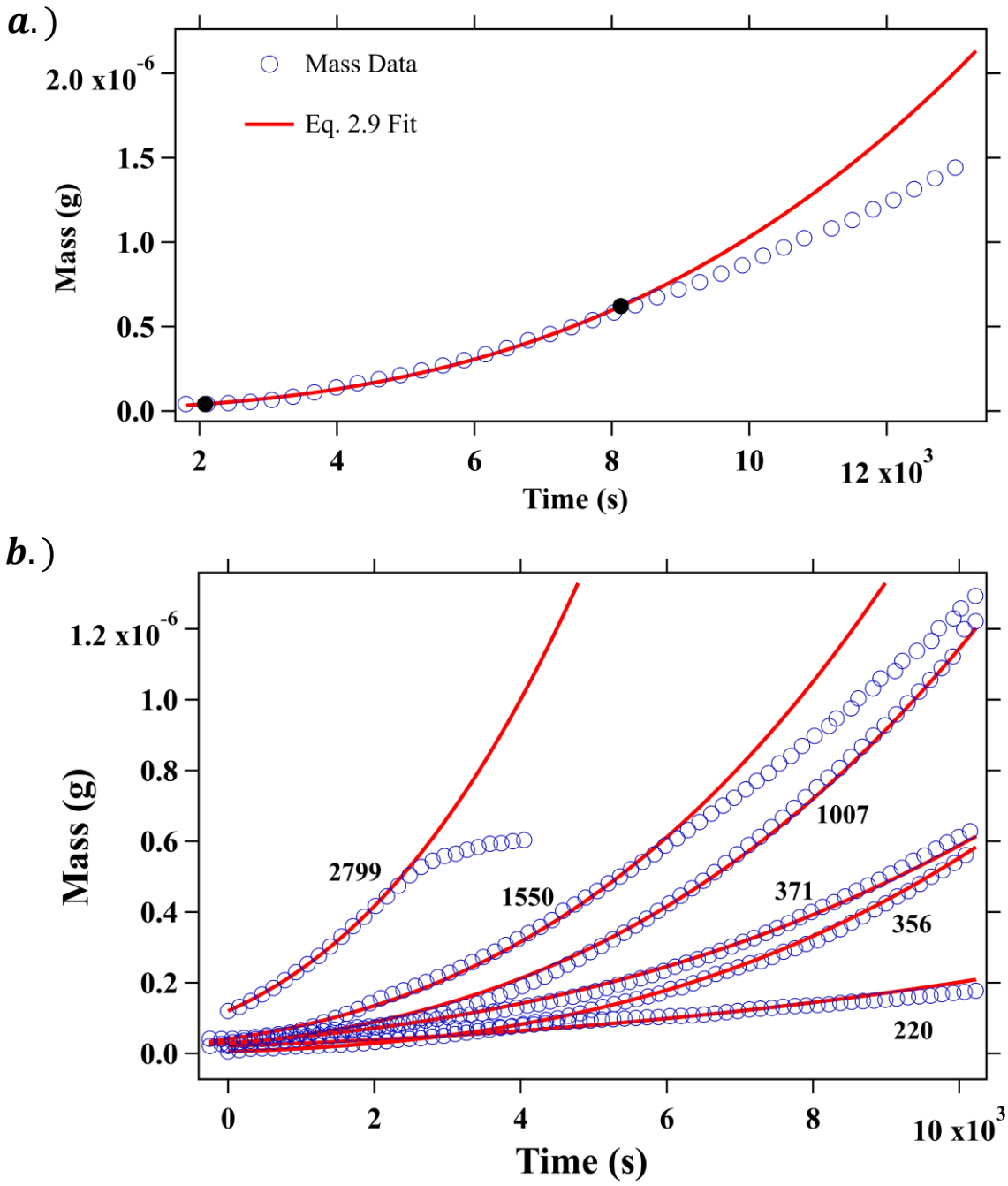

Figure 4.1: (a) Undriven growth of a seeded plate in $S = 12.5$ solution where $N = 1550$ and $m_0 = 41\ ng$. The red profile is the fit using Eq. 2.9, with $\bar{R} = 7.1\ \frac{\mu mol}{s \cdot m^2}$. (b) the fitted region of five additional data sets obtained under the same conditions, plotted alongside the first; the profiles are labelled with their respective N values.

These conclusions are contingent on the premise that N does not change during growth; if it did, the differential equation of Eq. 2.8 would not be solvable without knowing $N(t)$. Here we illustrate that N remains essentially constant during the growth phase. We have images our plates both before and after growth in order to determine the degree to which N remained constant. Figure 4.2 (a) shows the pre-growth image of a typical plate. Figure 4.2 (b) is an image of this plate following growth in an $S = 12.5$ solution (this is the same image as Fig. 3.3). In the post-growth image, 19 seeds have area values that exceed the area threshold value in our seed-counting algorithm. As can be seen, all of the 19 seeds present after growth were present before growth, demonstrating what we typically find; the seeds that contribute predominantly to the detected mass are formed in the nucleation phase. That said, there are more seeds present pre-growth than the 19 seeds encircled in the post-growth image. Thus, some seeds disappeared, perhaps detaching naturally or when transferring to growth solution. In addition, some of the seeds present after the seeding phase never grow significantly never grow significantly during the growth phase. However, as long as we accurately count the post-growth seeds *that grew* during the growth stage to get N, and verify that few or no *new* seeds form during growth, the pre-growth count is irrelevant.

a.)

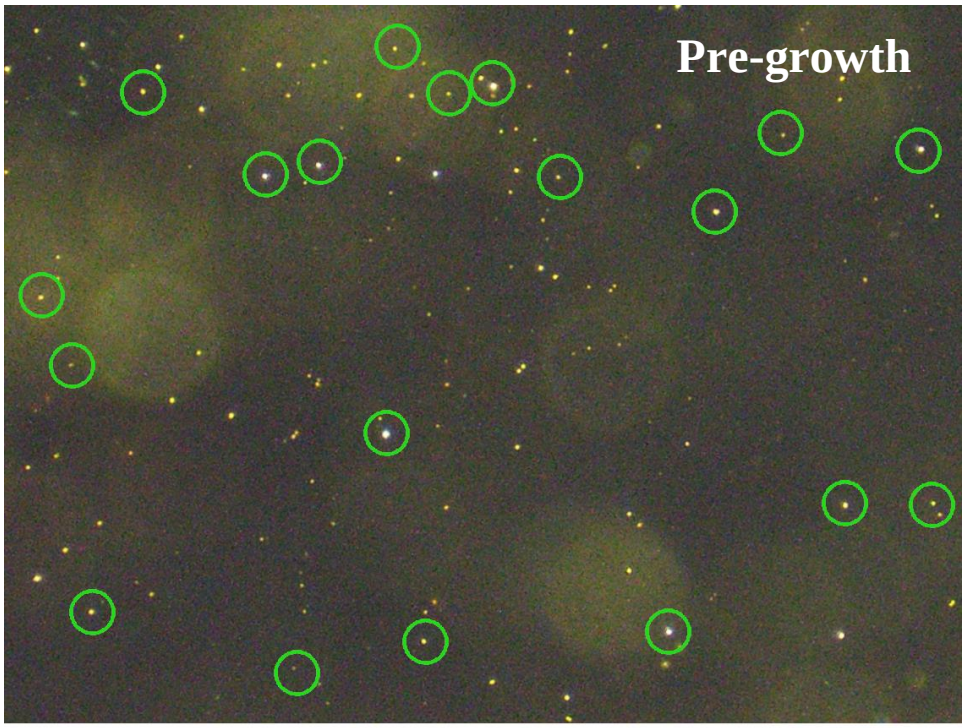

b.)

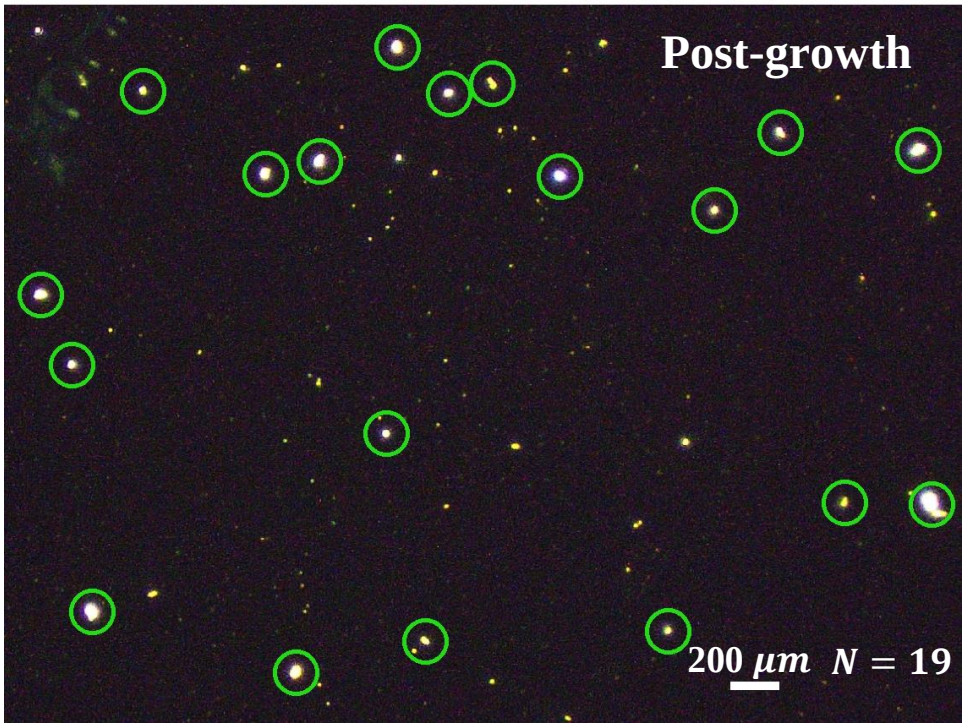

Figure 4.2: (a) A typical plate after seeding but before growth. (b) The same plate following growth in $S = 12.5$ solution.

4.2 Experimentally measured rates agree with prior research

Another key result is the agreement of measured undriven growth rates with prior research of calcite growth rates; these data are plotted alongside each other in Fig. 4.3. The red profile is data taken by Lammers and coworkers, who used a QCM with multiple attached crystals to measure growth rate - similar to this work. Measurements were made at supersaturations in the range $1.02 \leq S \leq 5.01$ [1]. The green profile is data from Teng et al., 2017; in this research, microscopic growth rates were measured *in situ* using atomic force microscopy to scan a growing calcite crystal. Measurements were made at supersaturations in the range $1.12 \leq S \leq 3.63$ [12]. The blue profiles are our data; the dark blue data are growth rates we collected in solutions with $14 \leq S \leq 74$. The light blue point is the average from the six growth rates for $S = 12.5$ solution, as seen in Fig. 4.1 (b); the 95% confidence interval is shown with error bars. The black line is a fit of all of this data to the theoretical relationship between growth rate and S: $\overline{R} = \alpha \cdot (\sqrt{S} - 1)$, where α is a constant. Our fit measured it to be $\alpha = 1.8 \pm .1 \frac{\mu mol}{s \cdot m^2}$, which is in agreement with prior work by Qiu and Orme which measured $\alpha = 1.83 \frac{\mu mol}{s \cdot m^2}$ [2].

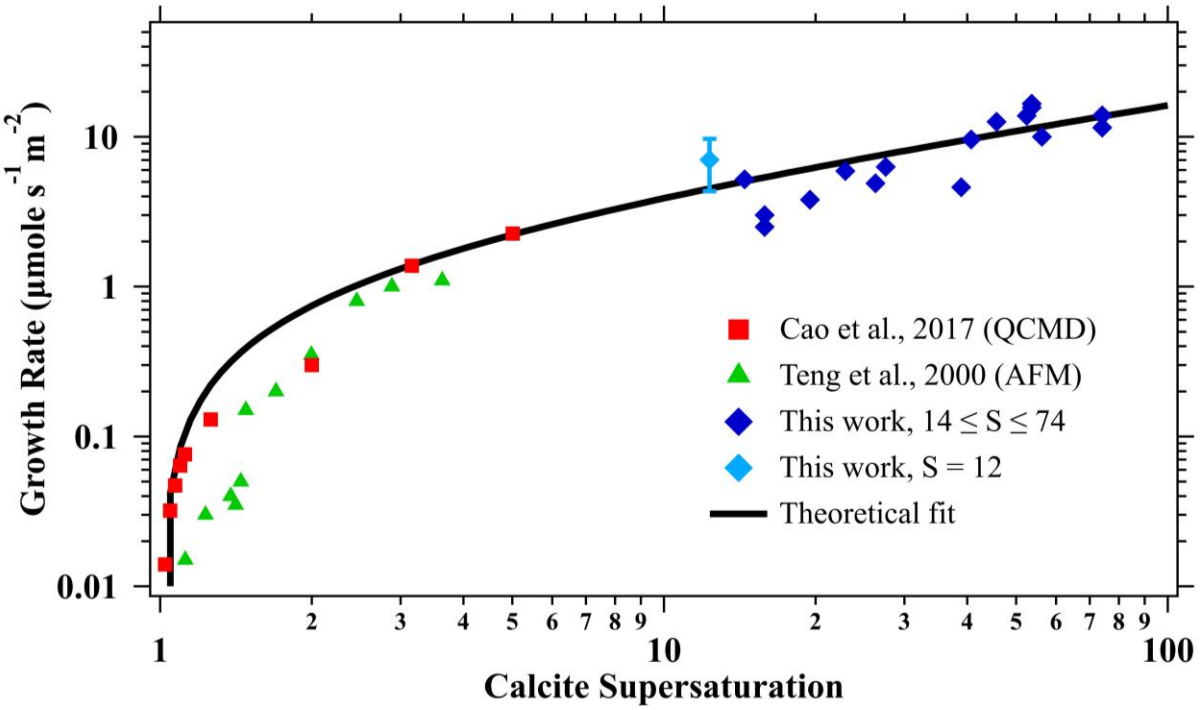

Figure 4.3: Calcite growth rates measured by various methods at various supersaturations; the data are fit to theory, $\overline{R} = \alpha \cdot \left(\sqrt{S} - 1\right)$ with $\alpha = 1.8 \pm .1 \ \frac{\mu mol}{s \cdot m^2}$, shown in black.

As can be seen, the data are largely consistent with each other and with the theoretical relationship across two orders of magnitude. Teng slightly less so than the others; however, it is still in notably good agreement, as it is a measurement on a completely different scale (AFM) to Cao and this work (QCM-D). It should also be noted that our work dealt with much higher supersaturations, and thus growth rates, than either Cao or Teng. This is another key finding: QCM-D with uniform beds of small seeds can be used to measure fast growth rates for which diffusive limitations are a complicating factor. However; as S is increased further, it becomes increasingly difficult to measure growth rates that are reaction-limited. This limitation holds implications for the measurement of driven growth, as discussed below.

4.3 This approach permits measurement of rapidly driven growth rates

We have found that our procedure is capable of measuring high growth rates, such as those found in potentiostatically-driven systems. Shown in Fig. 4.4 (a) is a typical data set for potentiostatically-driven growth, which was fit to Eq. 2.9 with $\bar{R} = 128\ \frac{\mu mol}{s \cdot m^2}$. This plate was seeded with $N = 1566$ seeds, with an initial total mass of $m_0 = 466\ ng$, and then electroprecipitated at an overpotential of $.613\ V$ in calcium-rich solution (details in Table 3.1). The resulting mass data are the blue circles, the fit of Eq. 2.9 is the solid red line, and the black circles mark the beginning and end of the region which we fit. As can be seen, the growth slows down much sooner than for the undriven case of Fig. 4.2 (a). Hence, we fit a commensurately shorter period: ~200 seconds versus ~4000 seconds, a difference of $20\times$! After this period, the growth becomes increasingly diffusion-limited and theory no longer describes the data. This behaviour matches our expectations, as the growth rates we are dealing with are on the order of $> 100\ \frac{\mu mol}{s \cdot m^2}$, over an order of magnitude larger than a typical undriven growth rate. Thus, the seeds should become diffusion-limited very quickly. Figure 4.4 (b) shows eight measured growth rates plotted versus overpotential, for driving voltages in the range $0 - 1.25\ V$. $\overline{R}$ scales with overpotential, and the linear fit was calculated to be $\overline{R} = 212 \cdot V + 4.5\ \ \frac{\mu mol}{s \cdot m^2}$. The right axis is in units of $4.5\ \frac{\mu mol}{s \cdot m^2}$, *i.e.* the amplification factor relative to the growth rate when driven at zero volts.

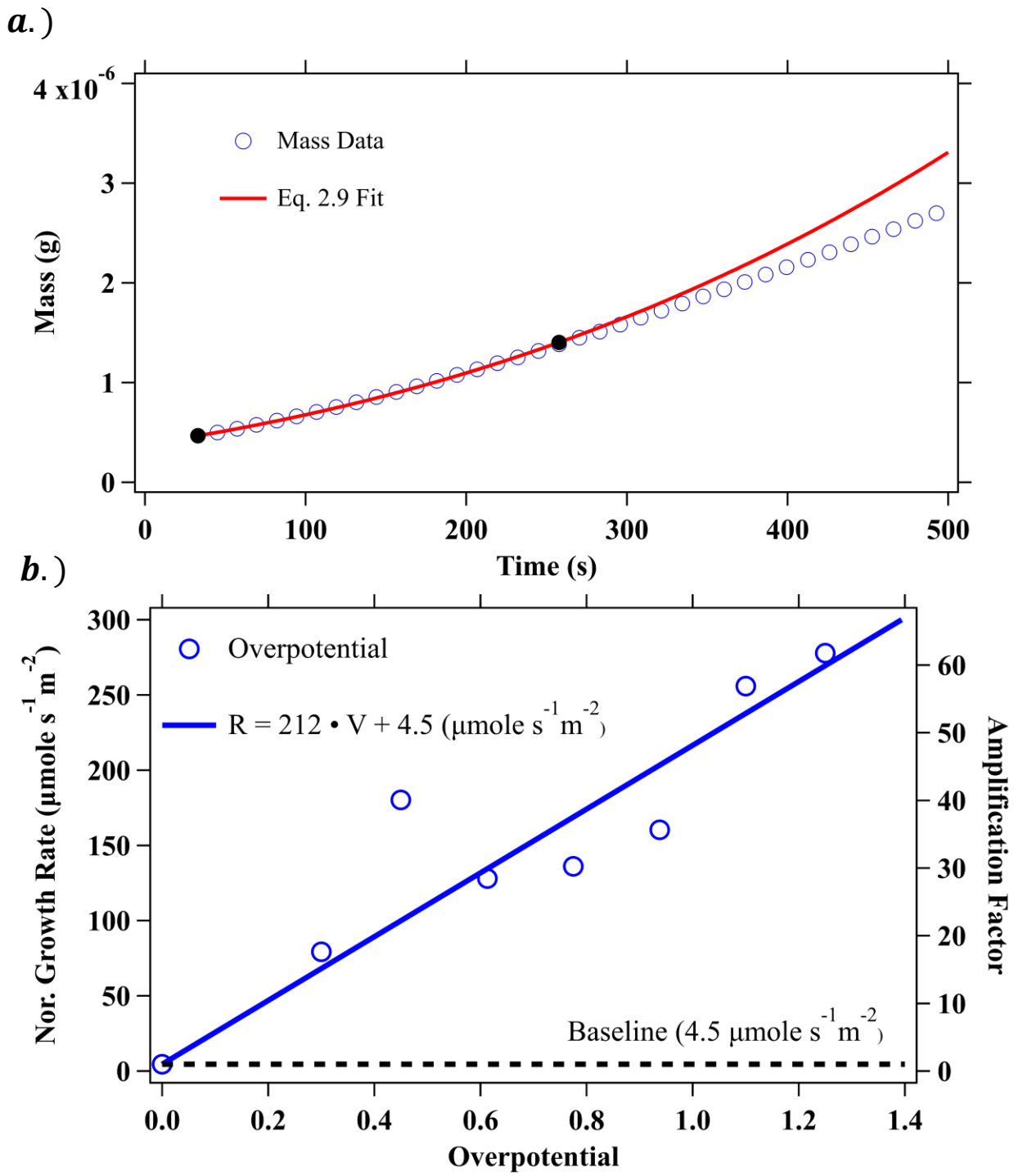

Figure 4.4: (a) Typical data set and fit for potentiostatically-driven growth, $\bar{R} = 128\ \frac{\mu mol}{s \cdot m^2}$. (b) Growth rate versus supplies overpotential for eight potentiostatically-driven data sets, with line of best fit.

4.4 Galvanic couples are powerful drivers of growth

We have found that galvanic couples are also powerful drivers of growth. Figure 4.5 (a) shows three datasets for stainless steel driven growth, which has an open circuit potential (OCP) of $0.4\,V$ relative to gold. The respective fits of these data are, from top to bottom: $\overline{R} = 113$, $\overline{R} = 110$, and $\overline{R} = 138$ in $\frac{\mu mol}{s \cdot m^2}$. These plates were grown in calcium-rich solution, as in table 3.1. In Fig. 4.5 (b), the growth rates of gold, copper, stainless steel, nickel, tin, cobalt, aluminum, lead, and zinc are plotted versus the measured open circuit potential (OCP) of that metal to gold, along with the potentiostatically-driven data from Fig. 4.4. As can be seen, growth rate is positively correlated to OCP, similar to $\overline{R}$ vs V for potentiostatically driven growth; this implies that OCP and overpotential play similar roles. These relationships may allow for the comparison of galvanic drivers to potentiostat voltages. Furthermore, by revisiting the theoretical fit in Fig. 4.3, we can extrapolate that relationship to calculate the supersaturation required to reach these growth rates. For instance, $\overline{R} = 100\,\frac{\mu mol}{s \cdot m^2}$ corresponds to S ~ 3000. Thus, properties of the solution at the interface, such as pH, can be gleaned from the resulting growth rates.

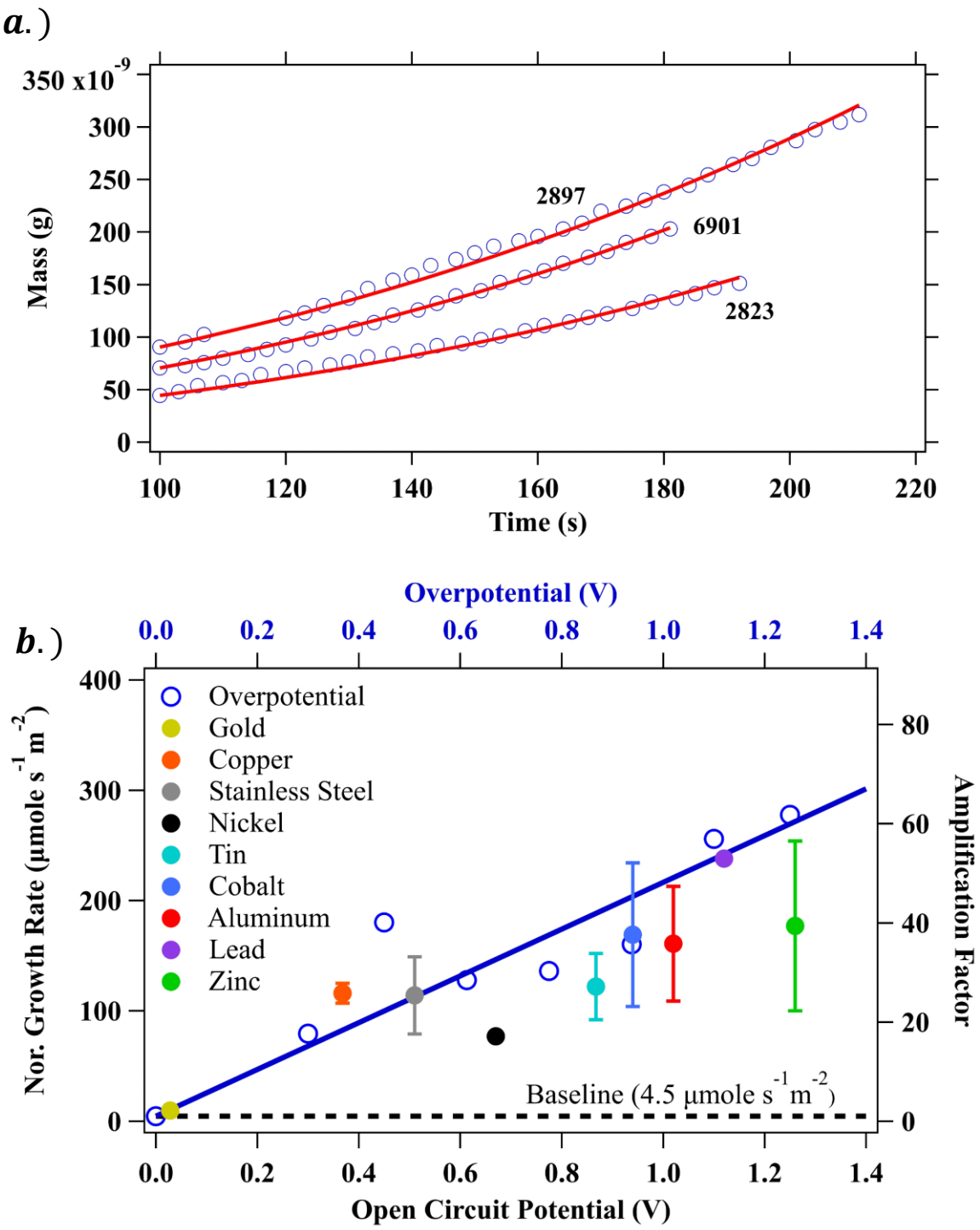

Figure 4.5: (a) three data-sets of growth driven by galvanic coupling to stainless steel. (b) $\overline{R}$ of growth driven by both an overpotential applied by a potentiostat (blue), as well as various galvanic couples

4.5 Galvanic couples drive mineralization in soil

Finally, we have found galvanic couples to be capable of driving the mineralization of carbonates in soil. A clean gold plate was placed in a soil-water solution (mud); The solution was made from deionized water mixed with calcium-rich soil, sourced from the Flint Hills of Kansas. An aluminum electrode was inserted, and connected to the gold via a wire. After 14 days, the gold was cleaned and imaged; this image is shown in Fig. 4.6 (a). There was a large amount of crystal on the surface, which effervesced when exposed to HCl, as would be expected for carbonates. Raman spectroscopy was performed on one crystal; the measured spectrum is shown alongside the calcite standard in Fig. 4.6 (b), confirming the crystal as calcite. Thus, we have shown the feasibility of driving calcite deposition in a soil sample using a galvanic couple.

a.)

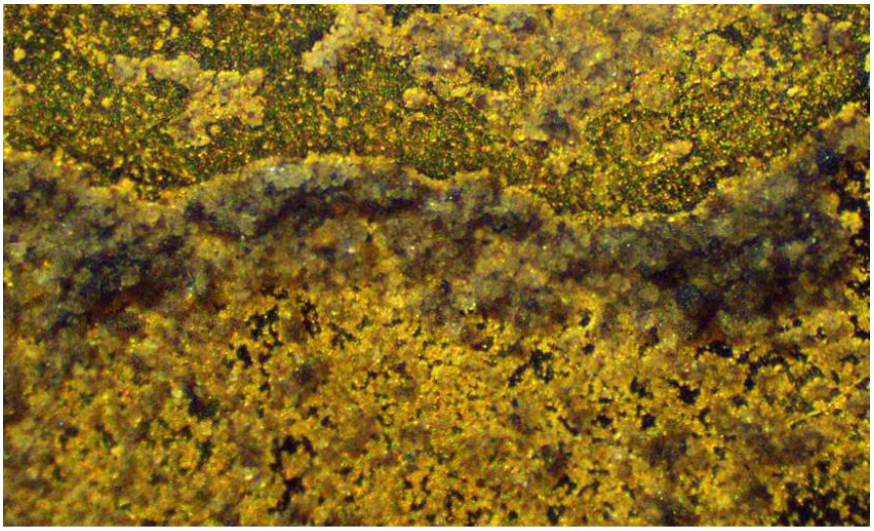

b.)

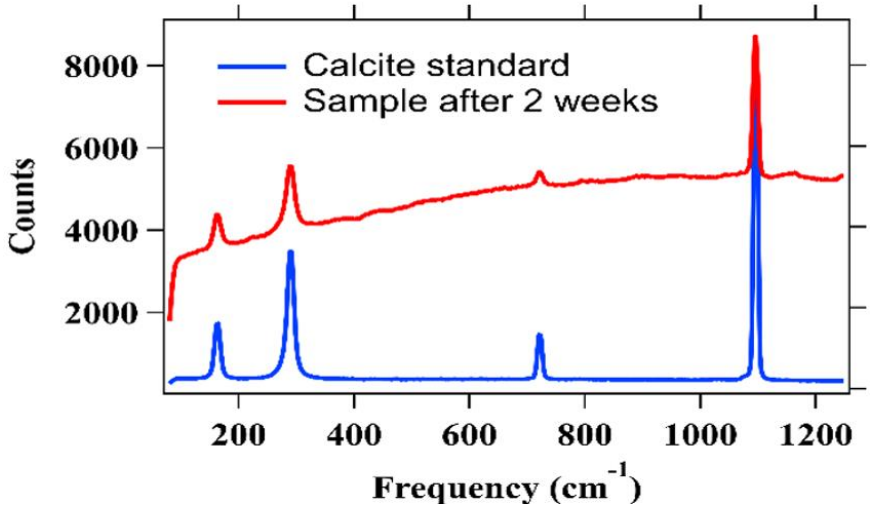

Figure 4.6: (a) A gold electrode after being submerged for two weeks in wet soil while galvanically coupled to aluminum. (b) Raman spectroscopy from a resulting crystal, alongside the standard spectrum for calcite.

Chapter 5

Conclusions

We have successfully used a quartz crystal microbalance in conjunction with a long working distance microscope to measure the growth of calcite. The observed $M(t)$ fits well to the predicted relationship between seed number, initial mass, and growth rate. We found that our measured growth rates agree with prior research [1][12], as well as the theoretical relationship between supersaturation and growth rate. We used a three-electrode system and potentiostat to induce the nucleation of seed beds of known N and mass. After placing these seed beds in solutions with various supersaturations to observe growth, N was found to have not increased, validating the use of a constant N when evaluating growth. We investigated the growth rates of seed beds under the influence of electroprecipitation, and found that galvanic couples and applied voltages are both powerful drivers of growth. Both are capable of driving growth at rates which are over an order of magnitude greater than the rate of undriven growth in that same solution. The fact that the resulting $M(t)$ still fits theory at early times indicates that this method is capable of measuring fast growth rates. The driven growth rate was found to be positively correlated to applied voltage in potentiostatic experiments; a linear fit yielded a slope of $212\ \frac{\mu mol}{s \cdot m^2}$ per volt applied. The galvanically driven growth rate was positively correlated to the galvanic cell's open circuit potential, indicating that open circuit potential may be analogous to driving voltage in potentiostatically driven growth. Finally, we have observed calcite to form on the gold electrode of a gold-aluminum galvanic cell when submerged in wet calcium-rich soil samples; this holds potential applications to carbon sequestration.

Bibliography

[1] B. Cao, A.G. Stack, C.I. Steefel, D.J. Depaolo, L.N. Lammers. Investigating calcite growth rates using a quartz crystal microbalance with dissipation (QCM-D). *Geochimica et Cosmochimica Acta*, vol. 222, Feb. 2018, pp. 269–283. URL https://doi.org/10.1016/j.gca.2017.10.020.

[2] S.R. Qiu, C.A. Orme. "Dynamics of biomineral formation at the near-molecular level." *Chemical Reviews*, vol. 108, no. 11, 12 Nov. 2008, pp. 4784–4822. URL https://doi.org/10.1021/cr800322u.

[3] J.B. Martin. "Carbonate minerals in the global carbon cycle." *Chemical Geology*, vol. 449, Jan. 2017, pp. 58–72. URL https://doi.org/10.1016/j.chemgeo.2016.11.029.

[4] N. Escoffier, P. Perolo, G. Many, N. Pasche, M. Perga. "Fine-scale dynamics of calcite precipitation in a large hardwater lake." *Science of The Total Environment*, vol. 864, Mar. 2023, p. 160699. URL https://doi.org/10.1016/j.scitotenv.2022.160699.

[5] B. Müller, J. Meyer, R. Gächter Müller. "Alkalinity regulation in calcium carbonate-buffered lakes." *Limnology and Oceanography*, vol. 61, no. 1, 19 Oct. 2015, pp. 341–352. URL https://doi.org/10.1002/lno.10213.

[6] R. Ramanan, K. Kannan, A. Deshkar, R. Yadav, T. Chakrabarti. "Enhanced Algal CO2 sequestration through calcite deposition by chlorella sp. and spirulina platensis in a mini-raceway pond." *Bioresource Technology*, vol. 101, no. 8, Apr. 2010, pp. 2616–2622, https://doi.org/10.1016/j.biortech.2009.10.061.

[7] B. Metz, O. Davidson, H. Coninck, M. Loos, L. Meyer (Eds.). *IPCC Special Report on Carbon Dioxide Capture and Storage*. Cambridge University Press, 2005. URL https://www.ipcc.ch/report/carbon-dioxide-capture-and-storage/

[8] T.O. Okyay, H.N. Nguyen, S.L. Castro, D.F. Rodrigues. "CO2 sequestration by Ureolytic microbial consortia through microbially-induced calcite precipitation." *Science of The Total Environment*, vol. 572, Dec. 2016, pp. 671–680. URL https://doi.org/10.1016/j.scitotenv.2016.06.199.

[9] M.L. Druckenmiller, M.M. Maroto-Valer, M. Hill. "Investigation of carbon sequestration via induced calcite formation in natural gas well brine." *Energy & Fuels*, vol. 20, no. 1, 25 Nov. 2005, pp. 172–179. URL https://doi.org/10.1021/ef050115u.

[10] R. Ramanan, K. Kannan, S. Sivanesan, S. Mudliar, S. Kaur, A. Tripathi, T. Chakrabarti. "Bio-sequestration of carbon dioxide using carbonic anhydrase enzyme purified from Citrobacter freundii." *World Journal of Microbiology and Biotechnology*, vol. 25, no. 6, 12 Feb. 2009, pp. 981–987. URL https://doi.org/10.1007/s11274-009-9975-8.

[11] P.M. Dove, M.F. Hochella. "Calcite precipitation mechanisms and inhibition by orthophosphate: In situ observations by Scanning Force Microscopy." *Geochimica et Cosmochimica Acta*, vol. 57, no. 3, Feb. 1993, pp. 705–714. URL https://doi.org/10.1016/0016-7037(93)90381-6.

[12] H.H. Teng, P.M. Dove, J.J. De Yoreo. "Kinetics of calcite growth: Surface processes and relationships to macroscopic rate laws." *Geochimica et Cosmochimica Acta*, vol. 64, no. 13, July 2000, pp. 2255–2266. URL https://doi.org/10.1016/s0016-7037(00)00341-0.

[13] M.M. Reddy, G.H. Nancollas. "The crystallization of calcium carbonate: I. Isotopic exchange and kinetics." *Journal of Colloid and Interface Science*, vol. 36, no. 2, 1971, pp. 166–172. URL https://doi.org/https://doi.org/10.1016/0021-9797(71)90161-5.

[14] M.M. Reddy, G.H. Nancollas. "The crystallization of calcium carbonate. II. calcite growth mechanism." *Journal of Colloid and Interface Science*, vol. 37, no. 4, Dec. 1971, pp. 824–830. URL https://doi.org/10.1016/0021-9797(71)90363-8.

[15] L.N. Plummer, T.M. Wigley, D.L. Parkhurst. "The kinetics of calcite dissolution in CO 2 - water systems at 5 degrees to 60 degrees C and 0.0 to 1.0 atm CO 2." *American Journal of Science*, vol. 278, no. 2, 1 Feb. 1978, pp. 179–216. URL https://doi.org/10.2475/ajs.278.2.179.

[16] L.N. Plummer, E. Busenberg. "A comparative study of the dissolution and crystal growth kinetics of calcite and aragonite." *Studies in Diagenesis*, vol. 1578, Jan. 1986, pp. 139–168. URL https://www.researchgate.net/publication/285267587_A_comparative_study_of_the_dissolution_and_crystal_growth_kinetics_of_calcite_and_aragonite

[17] J.N. Bracco, A.G. Stack, C.I. Steefel. "Upscaling calcite growth rates from the mesoscale to the macroscale." *Environmental Science & Technology*, vol. 47, no. 13, 20 June 2013, pp. 7555–7562. URL https://doi.org/10.1021/es400687r.

[18] J.N. Bracco, M.C. Grantham, A.G. Stack. "Calcite growth rates as a function of aqueous calcium-to-carbonate ratio, saturation index, and inhibitor concentration: Insight into the mechanism of reaction and poisoning by Strontium." *Crystal Growth & Design*, vol. 12, no. 7, 20 June 2012, pp. 3540–3548. URL https://doi.org/10.1021/cg300350k.

[19] E. Ruiz-Agudo, C.V. Putnis, C. Rodriguez-Navarro, A. Putnis. “Effect of ph on calcite growth at constant ratio and supersaturation.” *Geochimica et Cosmochimica Acta*, vol. 75, no. 1, Jan. 2011, pp. 284–296. URL https://doi.org/10.1016/j.gca.2010.09.034.

[20] A.G. Stack, M.C. Grantham. “Growth rate of calcite steps as a function of aqueous calcium-to-carbonate ratio: Independent attachment and detachment of calcium and carbonate ions.” *Crystal Growth & Design*, vol. 10, no. 3, 4 Feb. 2010, pp. 1409–1413. URL https://doi.org/10.1021/cg901395z.

[21] K. Larsen, K. Bechgaard, S.L.S. Stipp. “Modelling spiral growth at dislocations and determination of critical step lengths from pyramid geometries on calcite {} surfaces.” *Geochimica et Cosmochimica Acta*, vol. 74, no. 2, Jan. 2010, pp. 558–567. URL https://doi.org/10.1016/j.gca.2009.10.002.

[22] W. Stumm, J.J. Morgan. *Aquatic Chemistry: An Introduction Emphasizing Chemical Equilibria in Natural Waters*. Wiley, 1985.

[23] R. Phillips. *Physical Biology of the Cell*. CRC Press, 2012.

Appendix A –Python Code for seeding

```
# -*- coding: utf-8 -*-
"""
Created on Tue May  9 16:23:51 2023

@author: Ifland
"""

import matplotlib #Uncomment these two lines if you want a windowed graph or the code isn't
matplotlib.use('tkagg')

import pyvisa
import numpy as np
import matplotlib.pyplot as plt
import time
from numpy import savetxt
import cv2
from datetime               import datetime
from pygrabber.dshow_graph import FilterGraph
from os                     import path
import os
#import sys
import cv2 as cv
import keyboard
import string
import random
import sys
import glob

binary_threshold_input=150
minarea_input = 5
Experiment_Number = 1
QCMN = QCM_Number = 3
pause_time = .5
year_taken = "2023"

times = []
freq1s = []
absf1s = []
currents = []
VREs = []
CEs=[]
absr1s = []
r1s = []
counts = []

tinit= time.strftime("%d%H%M")
T0=time.time()
DEN = datetime.now().strftime("%y%m%d_")+ str(Experiment_Number)

BaseDirectory = 'S:/Flanders_Group/lab 12/Data/Current Data'
Image_Source_Path = r'S:/Flanders_Group/Flexacam'

initial_time_for_filenames = datetime.now().strftime("%Y_%m_%d-%I_%M_%S_%p_")
excel_file_name=path.join(BaseDirectory, str("Calcite Nucleation_" + DEN) +'.csv')
if path.isfile(excel_file_name)==True:
    sys.exit("That Excel already exists, change experiment and qcm number")
```

```
RF = 502
tname ="test plot"
OUTPUT_FOLDER         = BaseDirectory #I left this here so images *could* be stored somewh
CAMERA_INDEX          = 0 # Tells it which camera to use
n = 0 #counter used to give ordered integer values to image names
m = 0
error_count = 0
pad=4 #how many digits to pad the interger counter by

rm = pyvisa.ResourceManager()
rm.list_resources()
print(rm.list_resources())
fig = plt.subplot()
qcm1= rm.open_resource("ASRL7::INSTR") #Address for QCM controller

relay4 = rm.open_resource('ASRL4::INSTR')
relay4.write('3')

Nanovoltmeter = rm.open_resource('ASRL5::INSTR')
Nanovoltmeter.write(":*rst")
# relayN = rm.open_resource('ASRL9::INSTR')
# relayQCM = rm.open_resource('ASRL4::INSTR')

def channel1():
    Nanovoltmeter.write(":SENS:CHAN 1")
    Nanovoltmeter.write(":SENS:FUNC 'VOLT'")
    Nanovoltmeter.write(':SENS:VOLT:NPLC 1')
    Nanovoltmeter.write(":VOLT:DC:RANG 10")  # Range for nanovoltmeter


def channel2():
    Nanovoltmeter.write(":SENS:CHAN 2")
    Nanovoltmeter.write(":SENS:FUNC 'VOLT'")
    Nanovoltmeter.write(':SENS:VOLT:NPLC 1')
    Nanovoltmeter.write(":VOLT:DC:RANG 10")  # Range for nanovoltmeter


def nanoread():
    Nanovoltmeter.write(":READ?")




def grab_image():
    relay4.write('1')
    time.sleep(.15)
    relay4.write('3')
    #time.sleep(ptime)


#this function looks for the latest file in a certain location and opens it
def move_image(source_path,image_file_name):
    list_of_files = glob.glob(source_path + '/*.jpg') # * means all if need specific forma
    latest_file = max(list_of_files, key=os.path.getmtime)
    image = cv2.imread(latest_file)
```

```
    cv2.imwrite(image_file_name, image)



def Object_Count(original_image,binary_threshold_value,minarea):

    height = original_image.shape[0]
    width = original_image.shape[1]
    window_height = 999
    window_width = int((width/height)*window_height)
    #uncomment for full image
    top_pixel = 0
    bottom_pixel = height
    left_pixel = 0
    right_pixel = width

    #noise_range = 0
    connectivity = 4 #4 means pixels have to be directly adjacent on one of their four sides
    maxarea = 500000000
    cropped_original_image = original_image[top_pixel:bottom_pixel, left_pixel:right_pixel]
    #convert to greyscale
    gray_im = cv.cvtColor(cropped_original_image, cv.COLOR_BGR2GRAY)
    #Binary thresholding
    ret,binary_thresh = cv.threshold(gray_im,binary_threshold_value,255,cv.THRESH_BINARY)
    #count the objects
    output = cv.connectedComponentsWithStats(binary_thresh, cv.CV_32S, connectivity=connectiv
    (numlabels, labels, stats, centroids) = output

    highlighted_image = original_image.copy()

    n = 0
    for i in range(1, numlabels): #starts at 1 because 0 is the background
        # extract the connected component statistics and centroid for
        # the current label

        area = stats[i, cv.CC_STAT_AREA]
        (cX, cY) = centroids[i]


        if area >= minarea and area < maxarea:
            n = n+1 #count how many objects fit the criteria
            #highlight them on the background subtracted image
            cv.circle(highlighted_image, (int(cX+1), int(cY+1)), 10, (0, 0, 255), -1)

    return(n,highlighted_image,window_width,window_height)



def save_data():
    excel_file_name=path.join(BaseDirectory, str("Calcite Nucleation_" + DEN) +'.csv')
    savetxt(excel_file_name, np.transpose([times, freq1s, absf1s, r1s, absr1s, counts]), \
    header = 't%s_%s, f%s_%s, absf%s_%s, r%s_%s, absr%s_%s, N%sx_%s' \
    #header = 't2_%s, f2_%s, absf2s%s, r2s%s, absrs2%s, N2x_%s'
        %(QCMN, DEN, QCMN, DEN,QCMN, DEN,QCMN, DEN,QCMN, DEN,QCMN, DEN),fmt='%1.9f',delimiter
    graph_file_name=path.join(BaseDirectory, str("Calcite Nucleation_" + DEN) +'.jpg')
```

```
    plt.savefig( graph_file_name, format='jpeg', dpi=200, bbox_inches='tight',fmt='%1.9f')


def plot_data(t,f,N):

      ax1 = plt.subplot(3,1,1)
      ax1.plot(times, freq1s, color="blue")
      ax1.set_xlabel('Time (s)',fontsize=20.0)
      ax1.set_ylabel('f_1 (Hz)', color='blue',fontsize=20.0)
      ax1.autoscale()
      ax1.tick_params(axis='both', which='major', labelsize=30)
      ax1.ticklabel_format(axis='both', style='sci', scilimits=(-2,2))
      ax1.set_ylim()
      ax1b = ax1.twinx()
      print(counts)
      ax1b.plot(times, counts, color="green")
      ax1b.set_ylabel('N', color='green',fontsize=20.0)
      ax1b.autoscale()
      ax1b.tick_params(axis='y', labelcolor="green")
      plt.suptitle('t = %s s   f = %s Hz' %(round(t,0),round(f,0)),x=0.5,y=0.95,color='red',f
      plt.title('%s' % tname,fontsize=11)

      ax2 = plt.subplot(3,1,2)
      ax2.plot(times, r1s, color="blue")
      ax2.set_xlabel('Time (s)',fontsize=20.0)
      ax2.set_ylabel('r_1 (Ohms)', color='blue',fontsize=20.0)
      ax2.autoscale()
      ax2.tick_params(axis='both', which='major', labelsize=30)
      ax2.ticklabel_format(axis='both', style='sci', scilimits=(-2,2))
      ax2.set_ylim()

      ax3 = plt.subplot(3,1,3)
      ax3.plot(times, currents, color="blue")
      ax3.set_xlabel('Time (s)',fontsize=20.0)
      ax3.set_ylabel('Current (A)', color='blue',fontsize=20.0)
      ax3.autoscale()
      ax3.tick_params(axis='both', which='major', labelsize=30)
      ax3.ticklabel_format(axis='both', style='sci', scilimits=(-2,2))
      ax3.set_ylim()



      plt.show()

      save_data()

      plt.pause(.25)
# INITIAL READINGS
# relayN.write('1')   # noise OFF
# relayQCM.write('3') # qcm outer sleeve ON--breaks current carrying path
time.sleep(.5)
qcm1.write('P1')
absf10 = float(qcm1.query('F'))
qcm1.write('G')
absr10 = float(qcm1.query('R'))
time.sleep(.5)
# relayQCM.write('1') # qcm outer sleeve OFF--establishes current-carrying circuit through th
```

```
time.sleep(.5)
# relayN.write('3')   # noise ON

t20 = time.time()
count = 0

while True:
    while True:
    #while ( m == n ):
    #for i in range(1000000):

        channel1()
        nanoread()
        Vout = float(Nanovoltmeter.read())
        print(Vout*1000)
        current = Vout/RF

        channel2()
        nanoread()
        VRE = float(Nanovoltmeter.read())

        grab_image()
        time.sleep(.25)          # wait for camera to take pic
        tdata = time.time()-t20
        absf1 = float(qcm1.query('F'))  # read frequency
        freq1 = absf1-absf10
        absr1 = float(qcm1.query('R'))
        r1 = absr1 - absr10
        n = n + 1
        image_file_name = path.join(OUTPUT_FOLDER, str("img" + "_%s_" + datetime.now().strf
        time.sleep(.25)

        if keyboard.is_pressed("q"):
            binary_threshold_input=binary_threshold_input+10
            time.sleep(1)
        if keyboard.is_pressed("a"):
            binary_threshold_input=binary_threshold_input-10
            time.sleep(1)
        if keyboard.is_pressed("w"):
            minarea_input=minarea_input+1
            time.sleep(1)
        if keyboard.is_pressed("s"):
            minarea_input=minarea_input-1
            time.sleep(1)



        time.sleep(pause_time)
        move_image(Image_Source_Path,image_file_name)
        #time.sleep(pause_time/2)


        times.append(tdata)
        freq1s.append(freq1)
        absf1s.append(absf1)
        absr1s.append(absr1)
        r1s.append(r1)
```

```
        currents.append(current)
        VREs.append(VRE)
        counts.append(count)

        plot_data(tdata,freq1,count)
        original_image = cv2.imread(image_file_name)


        count,highlighted_image,window_width,window_height = Object_Count(original_image,bi
        print("filtered count:")
        print(count)
        print("binary threshold:")
        print(binary_threshold_input)
        print("minimum area:")
        print(minarea_input)



        labelled_highlighted_image = cv2.putText(highlighted_image, 't = %s s    f = %s Hz
        labelled_original_image = cv2.putText(original_image, 'frame #: %s    t = %s s    f =

        cv.namedWindow("original image", cv.WINDOW_NORMAL)
        cv.namedWindow('Hightlighted Features', cv.WINDOW_NORMAL)
        cv.resizeWindow("original image", window_width, window_height)
        cv.resizeWindow('Hightlighted Features', window_width, window_height)
        cv.moveWindow("original image",0,0)
        cv.moveWindow('Hightlighted Features', 0,0)
        cv.imshow("original image",labelled_original_image)
        cv.imshow('Hightlighted Features', labelled_highlighted_image)

        cv2.waitKey(15)

    else:
        print("it happened")
```

Appendix B – Python code for growth

```
# -*- coding: utf-8 -*-
"""
Created on Wed Apr 25 12:14:11 2022

@author: sbrijal
"""

import pyvisa
import numpy as np
import matplotlib.pyplot as plt

import time
from numpy import savetxt
from datetime              import datetime
import string
import random
import sys
import pHmeter_serial
from os                    import path
from IPython import get_ipython
get_ipython().run_line_magic('matplotlib', 'qt')

#%matplotlib qt


Experiment_Number = 3
QCMN = QCM_Number = 2
NGR = 8.4
NN = 100
f0 = 0



times = []
freq1s = []
freq2s = []
absf1s = []
absf2s = []
currents = []
VREs = []
CEs=[]
absr1s = []
r1s = []
absr2s = []
r2s = []
freqths = []
pH1s = []

tinit= time.strftime("%d%H%M")
DEN = datetime.now().strftime("%y%m%d_")+ str(Experiment_Number)
T0=time.time()
BaseDirectory = 'S:/Flanders_Group/lab 11/Data/Current Data'  #'C:/Users/newlab/OneDrive/
DEN = datetime.now().strftime("%y%m%d_")+ str(Experiment_Number)
excel_file_name=path.join(BaseDirectory, str("Calcite Nucleation_" + DEN) +'.csv')
if path.isfile(excel_file_name)==True:
    sys.exit("That Excel already exists, change experiment and qcm number")
```

```
RF = 502
delay_time = 10 #how long to pause in the data taking loop
EN = 1



rm = pyvisa.ResourceManager()
rm.list_resources()
print(rm.list_resources())
print(pHmeter_serial.list_serial_ports())
#fig = plt.subplot()

qcm1= rm.open_resource("ASRL4::INSTR") #Address for QCM controller
port = "COM12"

pHmeter_serial.configure_port(port)



def plot(t,f1,fTh,pH):


      plt.rcParams['figure.figsize'] = [10, 8]
      ax1 = plt.subplot(3,1,1)
      ax1.plot(times, freq1s, color="red")
      #ax1.plot(times, freq2s, color="blue")
      ax1.plot(times, freqths, color="black")
      ax1.set_xlabel('Time (s)',fontsize=14.0)
      ax1.set_ylabel('f_1 (red)', color='blue',fontsize=14.0)
      ax1.autoscale()
      ax1.tick_params(axis='both', which='major', labelsize=30)
      ax1.ticklabel_format(axis='both', style='sci', scilimits=(-2,2))
      ax1.set_ylim()
      plt.suptitle('t = %s s,  f = %s Hz,  fth = %s Hz\n\n pH = %s,  %s' %(round(t,0),round


      ax2 = plt.subplot(3,1,2)
      ax2.plot(times, r1s, color="red")
      ax2.set_xlabel('Time (s)',fontsize=14.0)
      ax2.set_ylabel('r_1 (Ohms)', color='blue',fontsize=14.0)
      ax2.autoscale()
      ax2.tick_params(axis='both', which='major', labelsize=30)
      ax2.ticklabel_format(axis='both', style='sci', scilimits=(-2,2))
      ax2.set_ylim()

      ax3 = plt.subplot(3,1,3)
      ax3.plot(times, pH1s, color="black")
      ax3.set_xlabel('Time (s)',fontsize=14.0)
      ax3.set_ylabel('pH_1', color='black',fontsize=14.0)
      ax3.autoscale()
      ax3.tick_params(axis='both', which='major', labelsize=30)
      ax3.ticklabel_format(axis='both', style='sci', scilimits=(-2,2))
      ax3.set_ylim()

      plt.tight_layout()
      plt.subplots_adjust(top=0.8)
```

```
        plt.pause(0.01)


qcm1.write('P1')


absf10 = float(qcm1.query('F'))
qcm1.write('G')
absr10 = float(qcm1.query('R'))

t20 = time.time()

while True:
    tdata = time.time()-t20
    absf1 = float(qcm1.query('F'))
    freq1 = absf1-absf10
    absr1 = float(qcm1.query('R'))
    r1 = absr1 - absr10
    f_theory = -((1.57*10**(-16))*NN*(NGR*tdata)**3 + ((8.7*10**(-11))**2)*NN**(2/3)*(NGR*td
    pH1 = pHmeter_serial.measure_pH(port)

    times.append(tdata)
    freq1s.append(freq1)
    freqths.append(f_theory)
    absf1s.append(absf1)
    absr1s.append(absr1)
    r1s.append(r1)
    pH1s.append(pH1)


    plot(tdata,freq1,f_theory,pH1)

#two options are given for saving excel column names - uncomment whichever you wish.
    savetxt('%s/Growth kinetics_7mM_%s.csv' %(BaseDirectory, DEN), np.transpose([times, freq
    header = 't%s_%s, f%s_%s, absf%s_%s, r%s_%s, absr%s_%s, freqth%s_%s, pH%s_%s' \
        %(QCMN, DEN, QCMN, DEN,QCMN, DEN,QCMN, DEN,QCMN, DEN,QCMN, DEN,QCMN, DEN),delimiter=

    plt.savefig('%s/Growth kinetics_7mM_%s.jpg' %(BaseDirectory, DEN), format='jpeg', dpi=20


    time.sleep(delay_time)
```